

T-1941

SOLUTE EFFECTS DURING
CYCLIC CREEP

by

John L. Kirk, Jr.

ProQuest Number: 10782108

All rights reserved

INFORMATION TO ALL USERS

The quality of this reproduction is dependent upon the quality of the copy submitted.

In the unlikely event that the author did not send a complete manuscript and there are missing pages, these will be noted. Also, if material had to be removed, a note will indicate the deletion.



ProQuest 10782108

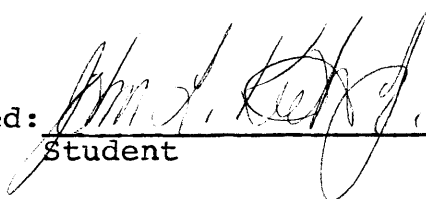
Published by ProQuest LLC (2018). Copyright of the Dissertation is held by the Author.

All rights reserved.

This work is protected against unauthorized copying under Title 17, United States Code
Microform Edition © ProQuest LLC.

ProQuest LLC.
789 East Eisenhower Parkway
P.O. Box 1346
Ann Arbor, MI 48106 – 1346

A Thesis submitted to the Faculty and Board of Trustees of the Colorado School of Mines in partial fulfillment of the requirements for a degree of Master of Science, Metallurgical Engineering.

Signed: 
Student

Golden, Colorado

Date: 4/15, 1977

Approved: 
Thesis Advisor


Head of Department

Golden, Colorado

Date: 15 April, 1977

ABSTRACT

In this thesis, the characteristics of cyclic creep acceleration of Al-4.6% wt.%Mg were studied in the temperature range of 318K ($0.37T_m$) to 358K ($0.42T_m$) at a peak stress of 237 Mpa. Cyclic creep acceleration is observed under these conditions.

The deformation behavior of Al-4.6%Mg for both static and cyclic creep was observed to result from normal creep processes in conjunction with intermittent propagation of inhomogeneous deformation bands, i.e. Luders bands. During creep, the propagation of Luders bands is evidenced by intermittent periods of increased strain rate.

The temperature dependence of the frequency of Luders band nucleation was found to be identical for both static and cyclic creep as well as Luders band initiation during standard tensile tests. This activation energy equals 74 kJ/mol. A possible mechanism with the proper activation energy is vacancy migration.

While the temperature dependence of the frequency of Luders band nucleation for both static and cyclic creep is equal, the frequency of Luders band nucleation for cyclic creep was characteristically faster than for static creep.

The result of the increased Luders band frequency was cyclic creep acceleration. A systematic increase in Luders band frequency was observed with increasing cyclic loading frequency.

The temperature dependence of static and cyclic creep rates was also determined by an average creep rate technique. The apparent activation energies for static and cyclic creep are 123 kJ/mol and 81 kJ/mol respectively.

The increased frequency of Luders band nucleation which results in cyclic creep acceleration is attributed to an increased rate of recovery occurring during cyclic loading. Two possible mechanisms, involving internal stress transients and excess non-equilibrium vacancies, are proposed to explain the enhanced recovery rate during cyclic creep.

TABLE OF CONTENTS

Abstract.....	iii
Table of Contents.....	v
List of Figures and Tables.....	vii
Acknowledgements.....	x
Chapter	
I. Introduction.....	1
Solid Solution Strengthening.....	3
Serrated Yielding.....	7
Low Temperature Creep of Al-Mg Alloys.....	17
Cyclic Creep.....	21
II. Experimental Procedure.....	25
III. Results.....	31
Strain Burst Characteristics.....	35
Temperature Dependence of Luders Band Nucleation During Creep.....	47
Analysis of Serrated Yielding by Tensile Tests.....	55
Analysis of Average Creep Rates.....	58

IV.	Discussion.....	66
V.	Conclusions.....	83
Appendix		
I.	Correlation of Random Variations in Static Strain Rate under Constant Conditions.....	85
	Literature Cited.....	88

LIST OF FIGURES AND TABLES

<u>Figure Number</u>	<u>Description</u>	<u>Page</u>
I-1	A schematic showing Type I and Type II serrations encountered in the dynamic strain aging temperature range during tensile testing.	8
I-2	The apparent creep activation energy as a function of temperature for Al-3%Mg (after Borch, Shepard and Dorn) and limited apparent activation energy data for static and cyclic creep of Al-4.6%Mg (after Rising).	18
II-1	A schematic of the experimental grip assembly used in creep and tensile tests.	27
II-2	A photograph of the experimental arrangement for a dual extensometer experiment.	29
III-1	A creep strain-time schematic of a mode change experiment.	32
III-2	Strain burst characteristics shown on a schematic of a portion of static and cyclic creep curves.	34
III-3	Strain-time as recorded by a diametral and a 1 inch axial extensometer during "steady state" creep. Test conditions: 332K, 237 Mpa, static loading, 1 inch gauge length.	38
III-4	Strain-time as recorded by a diametral, 1 inch axial and 2 inch axial extensometer during "steady state" creep. Test conditions: 322K, 237 Mpa, static loading, 2 inch gauge length.	40
III-5	A direct trace of experimental strain-time data from a cyclic dual extensometer experiment. Test conditions: 332K, 237 Mpa peak stress, 90% load	

<u>Figure Number</u>	<u>Description</u>	<u>Page</u>
	amplitude, 0.027 hz loading frequency (16 s hold time), 1 inch gauge length.	41
III-6	Comparison of average strain burst to strain burst observed after a smooth sample was scratched. Test conditions: 331K, 237 Mpa, static loading, 1 inch gauge length.	43
III-7	Diametral and 2 inch axial exten- someter strain-time trace during a "partial" propagating Luders band. Test conditions: 331K, 237 Mpa, static loading, 2 inch gauge length.	45
III-8	Temperature dependence of the frequency of Luders band nucleation during static creep at 237 Mpa.	49
III-9	Temperature dependence of the frequency of Luders band nucleation during cyclic creep at 0.027, 0.086, 0.132 hz and a peak stress of 237 Mpa.	50
III-10	A combination of Figures III-8 and III-9 showing the temperature depen- dence of Luders band nucleation during static and cyclic creep.	53
III-11	Temperature dependence of the initia- tion of Luders bands during tensile testing.	57
III-12	Temperature dependence of minimum static creep rates tested at a stress of 237 Mpa.	60
III-13	Temperature dependence of cyclic creep rates observed during mode change tests at a peak stress of 237 Mpa, 90% load amplitude and three loading frequencies.	61
IV-1	A schematic of stress and the resulting strain cycles observed during cyclic	

<u>Figure Number</u>	<u>Description</u>	<u>Page</u>
	creep. Included is the proposed internal stress transients.	74
IV-2	Strain-time data showing $\dot{\epsilon}$ upper controlled cyclic creep acceleration in high-purity aluminum. Test conditions: 348K, 37.2 Mpa peak stress, 80% load amplitude, 0.017 hz.	77
IV-3	A direct trace of strain-time data showing $\Delta \epsilon_p$ controlled cyclic creep acceleration in Al-4.6%Mg. Test conditions: 338K, 237 Mpa peak stress, 0.001 hz (500 s hold time), and three amplitudes.	78
IV-4	A comparison of high frequency of loading cyclic creep behavior (lower curve) to a low frequency of loading cyclic creep behavior (upper curve). Test conditions: 338K, 237 Mpa peak stress, 90% load amplitude, 0.027 hz-16 s hold time (lower curve) and 0.001 hz-500 s hold time (upper curve).	80
AI-1	The relationship between minimum static strain rate and instantaneous strain during loading observed in various creep experiments at 348K and 237 Mpa.	86

TABLES

<u>Table Number</u>	<u>Description</u>	<u>Page</u>
III-1	Average strain increment observed during strain burst at constant peak stress of 237 Mpa.	46
III-2	Apparent activation energy for cyclic creep between 318K and 358K at three frequencies. Obtained from Figure III-9	48
III-3	Summary of static and cyclic creep rates from mid range tests at 237 Mpa peak stress under various conditions.	64

ACKNOWLEDGEMENTS

I would like to thank Professor D. K. Matlock for his friendship, guidance, and encouragement throughout this investigation and my graduate studies.

I also wish to thank my wife, Jackie, for her continued support during my graduate studies.

I would like to express my thanks to Professors D. L. Olson, G. Krauss, G. Edwards, and W. L. Bradley for their valuable assistance and guidance.

Finally, I wish to acknowledge the Colorado School of Mines and the National Science Foundation for financial support during my graduate studies.

CHAPTER I

INTRODUCTION

Many material applications involve simultaneous creep and fatigue loading conditions. Design criteria using either pure fatigue or pure creep data have not proved satisfactory in predicting service lifetimes. Because of this, there currently is considerable effort directed toward the understanding of creep-fatigue interactions.

Approaches to the study of creep-fatigue interactions vary widely with investigators. The two most common methods of analysis are to consider a fatigue deformation process altered by creep stress, or to consider a creep deformation process altered by fatigue stresses. In this work, the latter of the suggested methods of analyses is used. In this thesis, static creep is defined as constant tensile load creep. The quoted stress is the true stress in the sample after the instantaneous elongation during loading. Comparisons are made between static and cyclic creep for cases where the peak cyclic load is equal to the corresponding applied static load.

Aluminum-4.6% Magnesium is the material used in this project. This alloy is similar in magnesium content to

several commercial aluminum alloys, 5083 and 5456. It is also of interest because it exhibits an enhanced cyclic creep rate compared to the static creep rate in the stress and temperature range to be studied.

The basic purpose of this thesis is to investigate and understand the mechanism of cyclic creep acceleration. This involves understanding the deformation behavior of this material in the stress-temperature range of interest and further understanding the effect of cyclic loading.

Prior to the presentation of the results of this thesis, the literature pertinent to the understanding of these results is reviewed. The specific subjects which are considered in the following sections are:

- (1) solid solution strengthening,
- (2) serrated yielding,
- (3) low temperature creep of Al-Mg alloys and
- (4) cyclic creep.

SOLID SOLUTION HARDENING

A brief overview of the principles of solid solution hardening and their application to the alloy under investigation is necessary to understand why there is interaction between solute atoms and dislocations. The four major factors related to the difference between solute and matrix atoms which effect solute-dislocation interactions are: (1) relative atomic size, (2) relative modulus, (3) electrical or valence, and (4) chemical. The driving force for solute-dislocation interaction is the sum of the interaction energies which result from these four factors. Qualitative discussions of the important interactions in the Al-Mg system follow. A complete review of solute-dislocation interactions can be found in a paper by Fiore and Bauer (1967).

The effect of lattice strain induced by the difference in atomic size between solute and solvent atoms provides the largest contribution to the total interaction energy. The difference in atomic size of magnesium, with an atomic radius of 1.60\AA , in aluminum, with an atomic radius of 1.43\AA , results in a 12% size difference. The relatively large size difference is the major factor in limiting the solid solubility of magnesium in aluminum to

14.9 weight %. Within the solid solution range, the size difference of the solute atom compared to the solvent atom forms a strain field around itself which interacts with the strain field associated with a dislocation. Edge dislocations produce both tensile and compressive hydrostatic strain field. Accompanying a larger solute atom, such as magnesium in aluminum, can reduce the strain if it diffuses to the tensile strain region of the dislocation. This strain reduction produce a decrease in the total strain energy of the system and thus the solute atoms interact with the dislocations.

To a first order approximation, screw dislocations have no hydrostatic component to their strain fields, which results in a much smaller interaction with solute atoms. In most substitutional solid solutions, Fiore and Bauer (1967) have shown that contributions of the size misfit to the total interaction energy is about 75% of the total interaction energy. The binding energy due to this size misfit is directly proportional to the relative size difference, the larger size difference, the larger the binding energy. In Al-Mg the binding energy would be expected to be quite large.

Differences in elastic modulus also cause solute-dislocation interactions. If the solute atom is softer,

that is more easily compressed than the matrix, then the energy of the dislocation strain field can be reduced by distorting the solute atom. This indicates that there will be an attraction between solute atoms with a lower elastic modulus and dislocations. The elastic modulus of magnesium, 6×10^6 psi, is only about half that of aluminum, 10×10^6 psi, which results in binding energy between magnesium atoms and dislocations.

Differences in electrical structure between solute and matrix atoms can also provide a contribution to the interaction energy. An electrical field is expected to exist around a dislocation from simple theoretical considerations. (Bauer and Fiore, 1967) All electron-energy theories relate the kinetic energy of an electron in a solid to the volume available for it to occupy. Since dislocations have strain fields associated with them, one would expect electrons to migrate from the tension side to the compression side of the field to lower the overall energy of the system. This migration results in a deficiency in charge in one region and an excess of charge in another region. The dislocation then acts like a line dipole and will interact with solute atoms possessing a net effective charge. Since magnesium (+2) and aluminum (+3) are of different valence states, one would expect

solute-dislocation interactions based on electrical considerations.

The final interaction to be considered is the chemical, sometimes called Suzuki, interaction. It is characterized by the attraction of solute atoms to stacking faults between dissociated dislocations. These solute atoms lower the stacking fault energy, which correspondingly increases the spacing between partial dislocations and increases the resistance to cross slip and climb. Prasad et al (1970) present arguments in their work that indicate Suzuki interaction does not occur in dilute Al-Mg alloys.

In summary, it is shown that the sum of the interaction energies due to relative size, relative modulus, and electrical considerations cause a potential difference between a solute atom in the matrix and a solute atom near a dislocation. This potential results in a driving force for the formation of solute atmospheres around dislocations. Bauer and Fiore (1967) calculate the binding enthalpy of zinc solute to a dislocation in copper to be about 18 kJ/mol (4.4 kcal/mol). It is anticipated that this energy is roughly comparable to magnesium in aluminum. This discussion showed, from theoretical considerations, an attraction will exist between

magnesium atoms and dislocations in dilute Al-Mg alloys. The following sections of this thesis will address the consequences of these interactions and their effect on cyclic creep.

SERRATED YIELDING

Serrated Yielding, jerky flow, or the Portevin-LeChatelier effect are names given a phenomena characterized by rapid increases and decreases in the flow curve of a material, as shown in Figure I-1. Many alloys exhibit serrated flow curves, notably steels in the blue brittle region (Baird 1971), Cu-Sn (Russell 1963, Ham and Jaffrey 1967), and Al-Mg (MacEwen and Ramaswami 1967, Brindley and Worthington 1969), as well as several aluminum alloys containing magnesium (6061-Reed-Hill et al 1975, Cetlin et al 1973, 6063-McCormick 1970, 1974, 1100-Rosen and Bodner 1966, Thomas 1966). Serrated yielding is the dynamic counterpart to a yield point or static strain aging phenomena. The jerkyness is attributed to successive yielding and aging which occurs as the sample is deformed. The jerkyness is sometimes called dynamic strain aging.

Theories attempting to explain serrated yielding fall into two broad categories, sudden dislocation motion and sudden dislocation generation. In the first category,

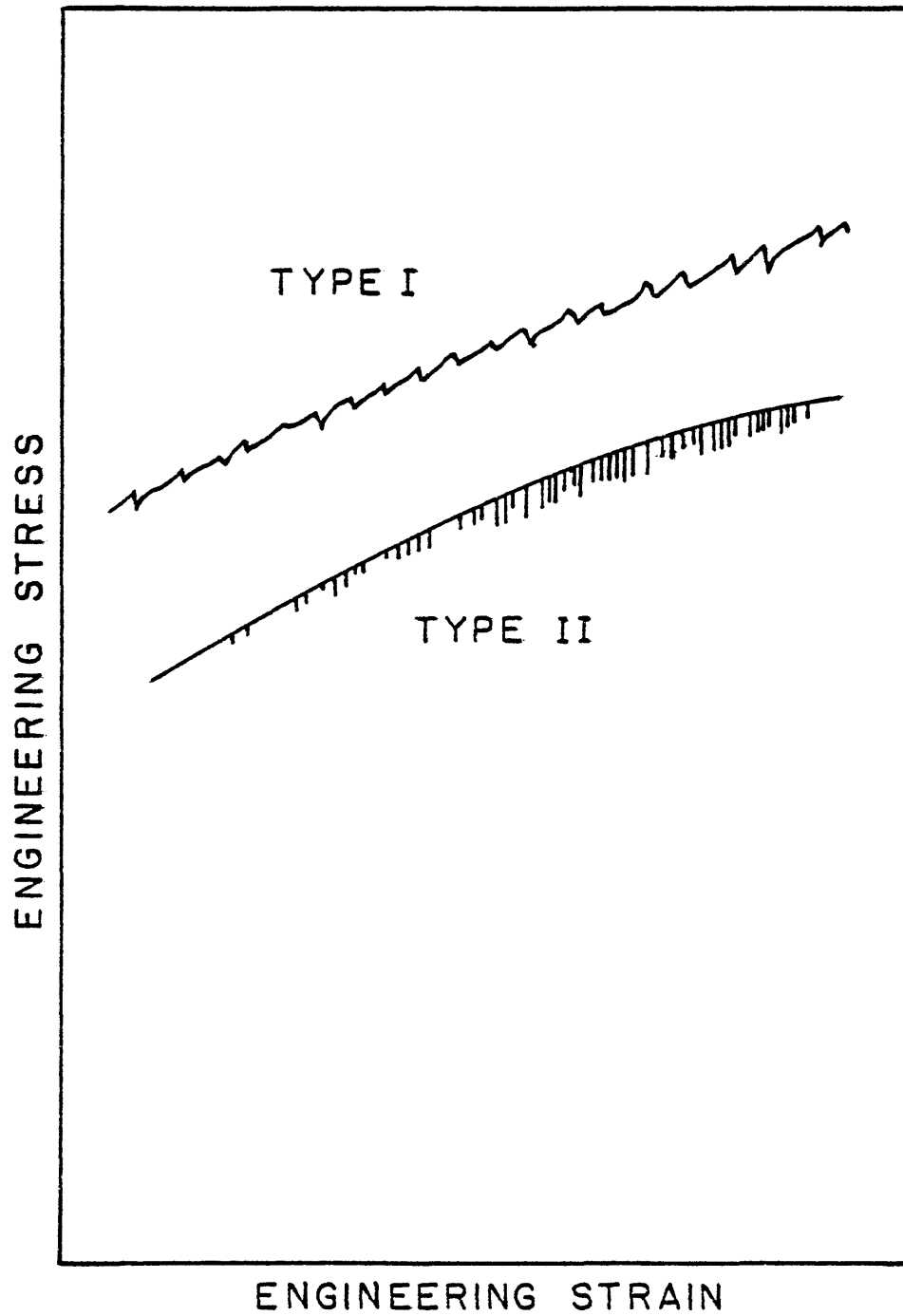


Figure I-1: A schematic showing Type I and Type II serrations encountered in the dynamic strain aging temperature range during tensile testing.

Cottrell (1953) proposed a theory based on solute atoms pinning dislocations and the subsequent dislocation break-away from these solute atmospheres. Cottrell explains the enhanced solute diffusivity necessary for the dynamic strain aging by the formation of excess vacancies during plastic flow.

Based on investigations of LiF single crystals, Johnston and Gilman (1959) explained yield points and serrated yielding as the sudden generation of new dislocations rather than motion of existing dislocations. While mechanisms have been proposed for sudden dislocation generation, no plausible explanation for the multiplicity of stress drops is given, nor an explanation for the strain rate or temperature dependence proposed.

Flow curve serrations were investigated by Mori and Meshii (1969) in quenched hardened aluminum single crystals. Slip bands with large initial displacements were the cause for these serrations. The mechanisms of local softening due to annihilation of loops and the rapid multiplication of mobile dislocations were proposed. The latter two theories, both in the category of sudden dislocation generation, are based on work involving single crystals. While generation of dislocations easily

explains the yield drop observed in single crystals, it has yet to be expanded to discuss the serrated flow behavior of polycrystalline materials.

The Cottrell theory is based on the requirement that dislocations and solute atoms move at essentially the same velocity through the lattice allowing constant interaction. For low temperature tensile tests, initially the dislocation velocity is much greater than the solute diffusivity, and there is no interaction. However, with strain, the average dislocation velocity will decrease due to changes in dislocation density and the diffusivity of the solute atoms increases due to increases in vacancies.

To describe sudden dislocation motion mathematically, expressions are necessary to relate plastic strain to the excess vacancy concentration, the excess vacancy concentration to the diffusion rate and finally to relate the diffusion rate to dislocation velocity and strain rate.

Seitz (1952) showed that excess vacancies can be formed by several mechanisms, such as the non-conservative motion of jogged screw dislocations. This non-equilibrium concentration of vacancies is described by the semi-empirical expression (Friedel 1964)

$$C_v = K\epsilon^m \quad (I-1)$$

where C_v is the excess vacancy concentration formed during plastic deformation, ϵ is the true strain, K and m are material constants.

The diffusion coefficient in a substitutional solid solution where diffusion is controlled by a vacancy-atom transfer mechanism can be written (Mulkherjee et al 1968)

$$D = AC_v \exp(-Q_m/RT) \quad (I-2)$$

where Q_m is the effective vacancy migration energy, A is a material constant, R and T are the gas constant and absolute temperature respectively. This relationship shows the interdependence of the diffusion rate and vacancy concentration. This statement assumes that the equilibrium thermal vacancy concentration is very small when compared to the excess vacancies formed during plastic flow and is neglected.

Cottrell described the critical dislocation velocity for dynamic strain aging as (Cottrell 1953)

$$V_c = 4D/\ell \quad (I-3)$$

where ℓ is the effective radius of the atmosphere. The critical dislocation velocity can now be related to a critical strain rate through the Orowan equation

$$\dot{\epsilon} = b\rho_m V_c = (4b\rho_m/\ell)D \quad (I-4)$$

where ρ_m is the mobile dislocation density and b is the

Burgers vector.

By combining the above equations, one obtains

$$\dot{\epsilon} = K \epsilon_s^m \rho_m \exp(-Q_m/RT) \quad (I-5)$$

where K is a material constant. This expression relates the important variables discussed by Cottrell; plastic strain, excess vacancy concentration, diffusivity, and dislocation velocity or strain rate. However, this critical strain rate expression, equation (I-5), is not complete as it does not include the variation in mobile dislocation density (Ham and Jaffrey 1967).

From experimental observations the mobile dislocation density, ρ_m , varies with plastic strain by (Ham and Jaffrey 1967, Johnston and Gilman 1959)

$$\rho_m = B \epsilon^\alpha \quad (I-6)$$

where B and α are material constants. Including this variation on the critical strain rate expression, the following is obtained,

$$\dot{\epsilon} = K' \epsilon_s^\beta \exp(-Q_m/RT) \quad (I-7)$$

where ϵ_s is the critical plastic strain for the onset of serrations, $\beta = (m + \alpha)$, and K' is a material constant.

Equation (I-7) can be rewritten as

$$\ln \dot{\epsilon} = K'' + \beta \ln \epsilon_s - Q_m/RT$$

One observes that the slope of the $\ln \epsilon_s$ versus $1/T$ at a constant $\dot{\epsilon}$ is equal to $Q_m/\beta R$. Plotting $\ln \dot{\epsilon}$ versus $\ln \epsilon_s$ at a constant temperature will yield a slope equal to β .

These two parameters, Q_m and β , are necessary to characterize the Potevin-LeChatelier effect based on the sudden dislocation generation mechanism as proposed by Cottrell.

Characteristics of serrations change with temperature within the dynamic strain aging temperature range. Two types of serrations are commonly reported in Al-Mg (Brindley and Worthington 1969, Thomas 1966, Mukherjee et al 1968, McCormick 1970). Type I occurs at lower temperatures and Type II occurs at higher temperatures. The temperature and strain rate dependence, flow curve characteristics, and possible explanations are discussed in the following paragraphs.

Type I serrations sometimes called Type A, periodic, or locking serrations are characterized by a sharp rise in stress above the flow curve followed by an immediate drop in stress below the flow curve as shown in stress-strain curve A of Figure I-1. These perturbations are attributed to a single Luders band propagating from one end of the sample to the other (Cetlin 1973). The critical strain before the initial serration has been found to increase with decreasing temperature and increasing strain rate (McCormick 1970, Brindley and Worthington 1969, Mukherjee et al 1968).

Type II serrations also called Type B, unlocking, or

fine serrations, shown in B of Figure I-1, are characterized by sudden, irregular stress drops below the level of the flow curve. Experimentally, each serration is described as the formation of a small non-propagating Luders band randomly over the gauge length. Many times these bands form ahead of one another (Cetlin et al 1973). This is called discontinuous propagation. In the case of Al-Mg, Type II serrations are seen just above room temperature (Brindley and Worthington 1969). A transition zone where characteristics of both types of serrations is also seen around room temperature. Strain rate and temperature dependence of the critical strain is opposite that of Type I serrations, increasing with increasing temperature and decreasing strain rate.

The negative strain rate dependence of Type II serrations is interpreted by McCormick (1970) as meaning the initial dislocation velocity is low enough for solute atmospheres to be dragged along with the dislocations. Therefore, the critical condition for the onset of serrations is the breakaway of dislocations from these existing atmospheres once the unlocking stress is reached. The breakaway explains the drop, rather than a rise, in the flow stress. In this region the atmosphere size also has a negative strain rate dependence, hence the higher

stress and resultant strain necessary for breakaway with increasing temperature.

In the lower region of the dynamic strain aging temperature range, McCormick suggests that solute atoms exhibit a diffusivity low enough such that initially the dislocations are unpinned. Serrations commence when the diffusivity of the solute is enhanced enough for solute atmospheres to form.

Thomas (1966) discusses an alternative description. In the upper region of the dynamic strain aging temperature range, where Type II serrations occur, dislocations are mostly pinned, The strain then is accommodated by the steady generation of new dislocations and their motion, rather than the breakaway of solute pinned dislocations. As the sample workhardens the stress required to form new dislocations approaches that to unpin old dislocations. The first jerk represents a catastrophic release of pinned dislocation.

A number of previous workers have investigated the strain rate and temperature dependence of both types of serrations in Al-Mg. Activation energies obtained from the plot of $\ln \dot{\epsilon}_s$ versus $1/T$ for Type I serrations have ranged from 25 kJ/mol (6kcal/mol) to 63 kJ/mol (15kcal/mol) and β values from 1.6 to 3.3 (Bindley and

Worthington 1969, Mukherjee et al 1968, Langdon and Mohamed 1973). For Type II serrations Mukherjee et al (1968) reported an activation energy of 77 kJ/mol (18.4 kcal/mol) and an β value of -2.88. Russell (1962) reported identical activation energies for Type I and II serrations in Cu-Sn and concluded activation by identical mechanisms. Considering the interdependence of the activation energy and β (that is the slope of the $\ln \dot{\epsilon}_s$ versus $1/T$ plot is $Q_m/3R$) the scatter in values is not surprising. An experimental value for the vacancy migration energy in aluminum is 63 kJ/mol (15 kcal/mol) (Brindley and Worthington 1969).

Several investigators have studied the effect of grain size on serrated yielding with inconsistent results. McCormick (1970) investigated the effect of grain size on serrations in a quenched commercial Al-Mg-Si alloy (6063) and concluded that the critical strain for the onset of serrations was independent of grain size. An explanation was proposed associating this behavior with solute supersaturation and possible strain induced precipitation. The transition temperature from Type I to Type II serrations was found to increase with increasing grain size.

In contrast to McCormick, an increase in activation energy with increasing grain size was observed in another

commercial aluminum alloy by Brindley and Worthington (1969). Coarse grained samples (0.6mm) resulted in a 54.4 kJ/mol (13 kcal/mol) activation energy compared to 41.8 kJ/mol (10 kcal/mol) for fine grained material (0.015mm). Mukherjee et al (1970) proposed an alternative analysis to Brindley's and Worthington's data that indicated no grain size dependence of the activation energy and calculated it to be 68.2 kJ/mol (16.3 kcal/mol). In this thesis, grain size was not varied making these inclusive results unimportant in this work.

LOW TEMPERATURE CREEP OF AL-MG ALLOYS

Several previous investigations have studied deformation mechanisms and creep of Al-Mg alloys in the low to moderate temperature range. A review of their results follows.

The temperature dependence of the creep activation energy in Al-3%Mg was investigated by Borch, Shepard and Dorn (1960) using temperature-change creep tests. Figure I-2, which shows the temperature dependence of the activation energy for creep, summarized their results. As shown, in region I, above 500K, the activation energy was found to be 149 kJ/mol (35.5 kcal/mol) which is the estimated value for self-diffusion in aluminum. Dislocation climb, a self diffusion controlled mechanism is hypothesized

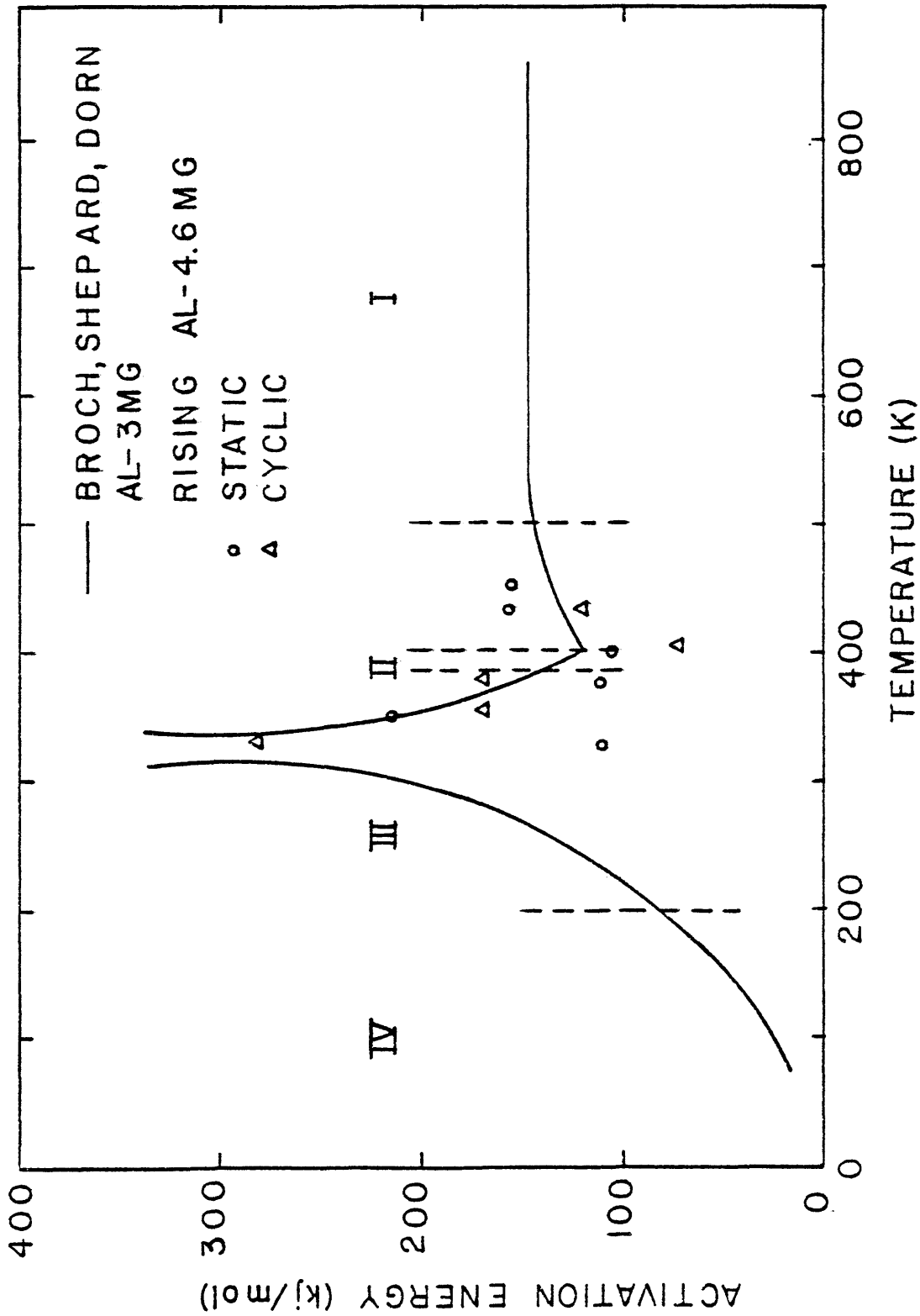


Figure I-2: The apparent creep activation energy as a function of temperature for Al-3%Mg (after Borch, Shepard and Dorn) and limited apparent activation energy data for static and cyclic creep of Al-4.6%Mg (after Rising).

based on this activation energy. An increasing activation energy, from 16 kJ/mol (4 kcal/mol) to 117 kJ/mol (28 kcal/mol), was found in region IV, 80 to 240K. This suggested a series of unresolved processes contributing to creep in this range. The apparent activation energy in region II, between 380 and 400K, was 117 kJ/mol (28 kcal/mol), which agrees well with the experimental activation energy for pure aluminum and theoretical predictions for the mechanism of cross slip. Region III, between 200 and 380K, exhibits a peak in the activation energy of over 335 kJ/mol (80 kcal/mol) at about 325K. This peak is rationalized in terms of Cottrell locking of dislocations by solute atmospheres. Borch, Shepard and Dorn propose that as dislocations approach a barrier they stop and remain at this barrier for some period of time before local energy fluctuations activate them past this barrier. If this waiting time is long enough, solute atmospheres will form and pin the dislocation. In the region of 325K, the waiting time at the barrier is long enough to form a completely saturated atmosphere such that thermal activation is not possible. Dynamic strain aging of Al-3%Mg at 325K is rationalized by stress concentrations raising the local stress high enough to athermally unlock the dislocations from their atmospheres resulting in a Luders band. The

activation energy in region III is concluded to be the sum of two parts, the activation energy for cross slip and the activation energy to free dislocations from their atmospheres.

Prasad, Sastry and Vasu (1970) investigated the mechanisms of deformation in various dilute Al-Mg alloys using tensile tests and stress-change creep tests. Around room temperature no measurable creep was reported in any of the alloys tested, while at lower and higher temperatures measurable creep occurred. Prasad et al conclude that in the higher temperature range, 373 to 423K, the effect of solute atoms on dislocation motion is not prominent. In the temperature range below 200K, several deformation mechanisms were considered. The conclusion indicating best agreement with the model of hardening by pinning of dislocations by randomly dispersed solute atoms. In the temperature region around room temperature, Prasad et al followed the lead of Borch, Shepard, and Dorn by describing athermal locking of dislocations by solute clouds as responsible for the negligible creep rates.

Sherby and Burke (1968) also reviewed the creep of Al-Mg. In contrast to previous investigators, they interpreted the peak in activation energy seen in region III to be a real activation energy for some thermally activated

process and do not consider an athermal process.

CYCLIC CREEP

Investigations into cyclic creep have revealed some unexpected, important results, namely cyclic creep acceleration. Cyclic creep acceleration occurs when the average cyclic creep rate is faster than the static creep rate at the same peak load. Conversely cyclic creep retardation occurs when the static rate is faster than the cyclic creep rate at equal peak loads. Studies in a wide variety of engineering materials including steels (Evans and Parkins 1976), aluminum alloys (Coutinho et al 1975, Shetty et al 1973), and superalloys (Organ et al 1971), reveal cyclic creep acceleration. Earlier work is reviewed in an article by Meleka (1962) and more recently in a dissertation by Coutinho (1973). While data has been gathered for a number of engineering materials, limited investigations of the basic mechanisms of cyclic creep acceleration are found. Discussions of major experimental work and theoretical modeling follow.

Kennedy (1956) conducted an early investigation in the subject of cyclic creep using lead at 305K. To explain the marked acceleration in creep rate after the introduction of a superimposed vibrational cyclic stress,

he suggested recovery was enhanced by the creation of excess vacancies during cyclic stressing.

An explanation of cyclic acceleration observed in copper at 623K using a sinusoidal stress function was proposed by Meleka (1962). In this work it was suggested that cyclic stressing increased the dislocation mobility and therefore caused cyclic acceleration.

More recently, Gibbons et al (1973) studied cyclic creep in nickel at 923 and 1023K using a low frequency square wave loading function. Cyclic retardation occurred in all cases. After studying each portion of the deformation cycle, they proposed that recovery did occur at the lower stress, but its magnitude was not sufficient to cause acceleration.

Shetty and Meshii (1973) investigated the cyclic creep behavior of high purity aluminum in the range of 77 to 295K using a carefully controlled trapezoidal loading function to avoid overshoot. They reported both cyclic acceleration and retardation depending on the combination of stress, temperature, amplitude, and prior static creep rate. Stress was observed to be the most important experimental variable, with increasing stress causing increasing acceleration. In further work, Meshii (1975) proposed a mathematical model predicting cyclic creep

behavior based on structural softening by more uniform plastic strain distribution brought about by load cycling. Reformation and modification of this model is discussed in further work (Shetty et al 1975).

Prior work in Al-4.6%Mg began with Coutinho (1973, Coutinho et al 1975) studying static and cyclic creep between 324 and 360K ($0.38-0.40T_m$). Stress dependence of static and cyclic creep was shown to be identical along with an average activation energy for cyclic creep of 142 kJ/mol (34 kcal/mol) in this temperature range. Cyclic acceleration was reported in this work at a stress level of 237 Mpa (34.4 Ksi). Recovery effects at the lower stress was given as the explanation of cyclic acceleration.

Nam (1974) investigated this same alloy by comparing static and cyclic creep rates in the range of $0.4-0.6T_m$ at a constant $\sigma(\epsilon_0)/E(T)$. Below $0.5T_m$ at this "constant" stress, cyclic acceleration was reported with the reverse being true above $0.5T_m$. At a constant $0.5T_m$, cyclic creep rates were faster than static in the higher stress regions and slower than static in the lower stress region.

Again using Al-4.6%Mg, Knaus (1975) studied the effect of stress function on fatigue-perturbed creep. Using a square wave function, the instantaneous strain upon

reloading, $\Delta\epsilon_p$, was defined and related to the amount of recovery at the lower stress. The effect of frequency, amplitude and temperature on recovery and $\Delta\epsilon_p$ was reported. A model based on internal stress transients was suggested.

Matlock and Bradley (1976) presented a similar, more complete internal stress transient model that qualitatively explains experimental results. Enhanced recovery occurring during unloading causes excess strain upon reloading or an increased strain rate at the upper stress, depending on material characteristics. Cyclic acceleration and retardation as well as variations in experimental conditions are qualitatively explained by this model.

The principles presented in this introduction will now be used to analyze the experimental results to be presented. Using these principles and present results, an explanation of cyclic creep acceleration will be proposed.

CHAPTER II

EXPERIMENTAL PROCEDURE

Aluminum-4.6 wt % Magnesium is the material used in this investigation. This alloy was specifically prepared by ALCOA for this project by vacuum casting 99.99% pure aluminum with proper additions of 99.99% pure magnesium. The material was then extruded into 1.9×10^{-2} m (.75") diameter rods which were fully annealed. Chemical analysis shows less than 0.01 weight % for each of the following: Si, Fe, Cu, Mn, Cr, Ni, Zn, Ti, Be; 4.61 weight % Mg and the balance Al. Round, reduced-section tensile samples were machined from the extruded rod. Two similar geometries were tested: (1) 0.0250 inch diameter by 1.0 inch nominal gauge length, (2) 0.250 inch by 2.0 inch nominal gauge length. The machined samples were annealed in a Varian Marshall tube furnace (model #1039) for 3900s (65 minutes) at 623 ± 2 K. The anneal was performed under a vacuum of approximately 5×10^{-4} torr. Samples were air cooled. This resulted in a uniform grain size of 0.246mm.

An MTS Model 810 electro-hydraulic closed-loop testing system was used in all experiments. The majority

of tests reported were run using the grip and strain measurement system shown in Figure II-1. Oil (HTE-100 UCON) was heated in a Blue M constant temperature bath (model #MW-1145A-1) and circulated through the dewar to control sample temperature. Sample temperatures were maintained within 0.5K with this apparatus.

With the gripping assembly shown in Figure II-1, the extensometer was used to measure total sample elongation. This elongation was then converted to strain using an effective gauge length. In earlier work (Knaus 1975) using this gripping assembly, the effective gauge length was determined to be 0.03048m (1.2 inches) by conducting a slow strain rate tensile test and correlating actual sample strains to grip displacement.

This effective gauge length was checked and subsequently modified using the following relationship

$$l_o = \frac{\Delta l (A_f)}{A_o - A_f} \quad (\text{II-1})$$

where Δl is the total elongation, A_f is the final area, A_o is the initial area and l_o is the effective gauge length. Calculation of effective gauge length from test data indicated a better average value to be $0.0279 \pm .0013\text{M}$ ($1.1 \pm .05$ inches). This value was used in strain calculations throughout this work.

Strain-time and load-strain were continuously recorded

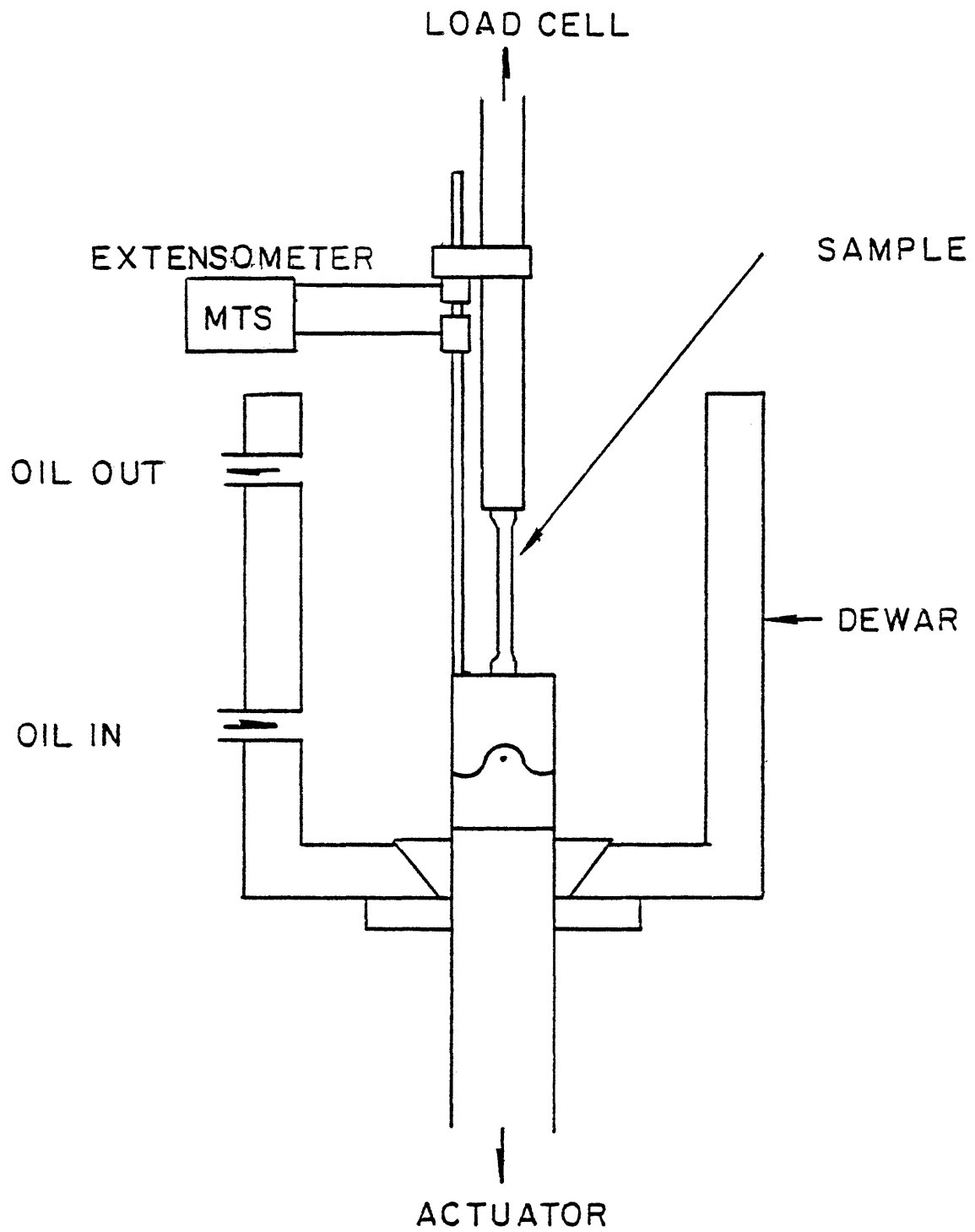


Figure II-1: A schematic of the experimental grip assembly used in creep and tensile tests.

using an MTS model 632.12 extensometer and an MTS model 661.21 A-01 load cell (5,000 pound capacity). Strain was measured to an accuracy of 1×10^{-4} and load was maintained within 1.1N (0.25 pounds) during a test.

Some experiments were conducted using two extensometers, an axial and a diametral shown in Figure II-2. These tests were performed in a specially designed foil-lined box mounted on the crosshead using incandecent light bulb for heating. Temperature control during these tests was $\pm 3K$. Diametral measurements were made using an MTS model 632.19B extensometer excited through an MTS conditioner. Measurements were accurate to within 2×10^{-4} . Axial strain was measured with an MTS model 632.11 extensometer excited with a storage battery. Experiments were performed measuring both grip displacement and also directly measuring strain on the sample. Axial creep strains could be measured to an accuracy of 8×10^{-6} using these methods.

All creep tests were run in load control using a controlled loading rate trapezoidal wave form. This waveform was used to approximate a square wave, but insured no load overshoot would occur. A loading rate of 550 pounds/second was used throughout all experiments. Stress values quoted are the true stress after the instan-



Figure II-2: A photograph of the experimental arrangement for a dual extensometer experiment.

taneous strain during loading. Actual stress values are within $\pm 2\%$ of the nominal values.

Tensile tests reported in this work were also run using the grip assembly shown in Figure II-1. These experiments were run in strain control using a ramp function. Load-elongation was recorded as with creep tests.

CHAPTER III

RESULTS

The following sections present the results of the experimental program. This experimental program was designed to investigate the effect of the solute in Al-4.6%Mg on cyclic creep acceleration. Results from experiments are divided into four categories: (1) experimental evidence of Luders bands during creep, (2) the temperature dependence of Luders band nucleation during creep, (3) analysis of serrated yielding by tensile tests, and (4) analysis of average creep rates.

All cyclic creep data discussed in this thesis was derived from mode change experiments. As shown in Figure III-1 a mode change test consists of an initial portion of static creep, followed by cyclic creep. Ideally, the point at which loading modes are changed from static to cyclic is the point of minimum static strain rate. However, time constraints at low-temperatures made this mode change point unrealistic. In these cases, the mode change was made as late in primary creep as possible within time constraints.

A short transient during the early portion of cyclic

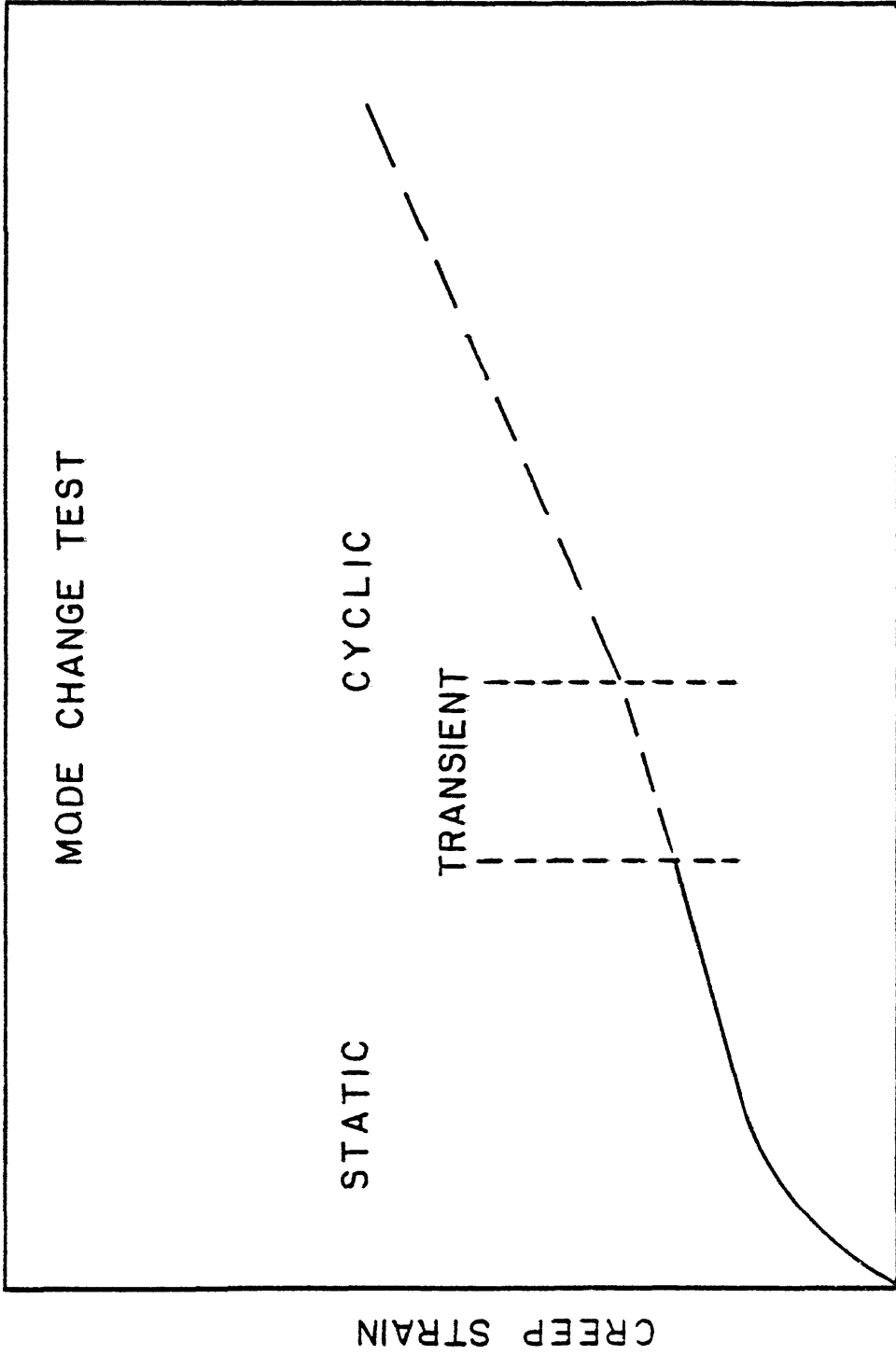


Figure III-1: A creep strain-time schematic of a mode change experiment.

creep was observed after the mode change as shown in Figure III-1. All cyclic measurements were made after this transient.

The true stress after the instantaneous elongation which occurred during loading was held constant for all static and mode change creep tests at 237 ± 5 Mpa (34.4Ksi). Cyclic load amplitude was also held constant at 90% for the cyclic portion of all experiments. A 90% load amplitude means the lower stress was 24 Mpa when the peak stress equaled 237 Mpa.

Figure III-2 shows typical static and cyclic strain-time behavior of Al-4.6%Mg in the temperature range of interest. Both static and cyclic creep are characterized by the intermittent strain bursts shown in Figure III-2. Extensive analysis of the phenomena of strain bursts is included in this thesis. In order to easily discuss the subject, several definitions are necessary. First, the fluctuations in the strain rate observed in the creep curve, as shown in Figure III-2, will be called strain bursts. The average time for one strain burst cycle, is defined as the total time, t_t . The strain burst frequency is simply the inverse of total time. The strain occurring during t_t , ϵ_t , is divided into two parts. ϵ_c is the "normal" creep strain between strain

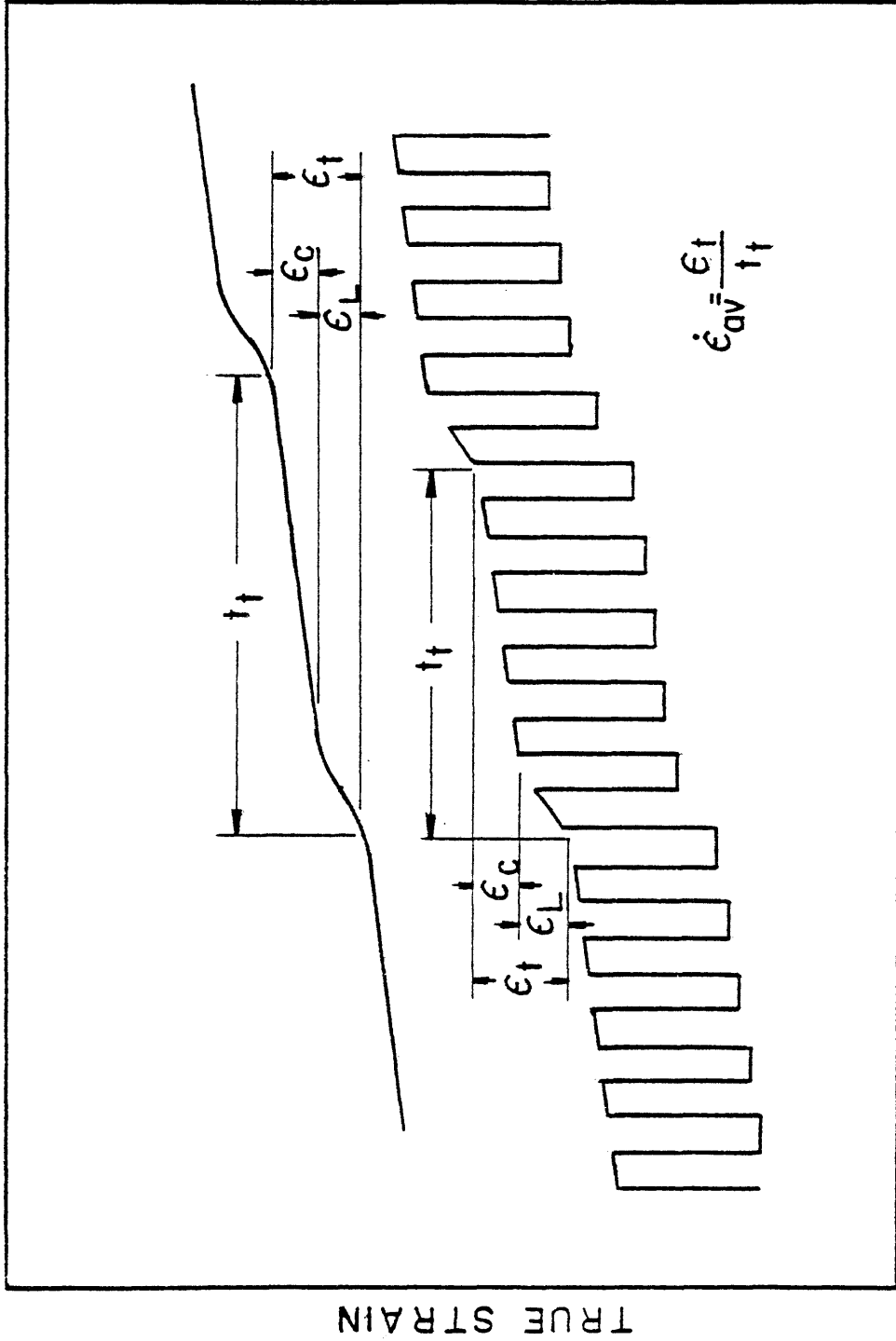


Figure III-2: Strain burst characteristics shown on a schematic of a portion of static and cyclic creep curves.

bursts, and ϵ_L is the strain occurring during a strain burst. The average strain rate is found by dividing the total strain, ϵ_t , by the total time, t_t . The first section of this chapter will discuss the characteristics of the strain bursts.

STRAIN BURST CHARACTERISTICS

As mentioned previously, the strain-time behavior of Al-4.6%Mg at moderate temperatures is characterized by regular bursts of strain evidenced by a rapidly changing strain rate (see Figure III-2). Under static loading, the strain bursts are observed in a narrow temperature range, between 318 and 338K (0.37 to $0.4T_m$). Static strain bursts are characterized by fairly regular intervals of increased strain rate. As temperature decreases, the frequency of strain bursts also decreases and becomes less regular.

Creep under cyclic loading conditions also exhibits strain bursts, but in a slightly wider temperature range, 318K ($0.37T_m$) to 358K ($0.42T_m$). Strain bursts during cyclic creep exhibit similar general characteristics as those observed during static creep with two important variations. First at constant temperature, the frequency of cyclic strain bursts is faster than static strain bursts.

Secondly, cyclic strain bursts are more regular than static strain bursts in the lower temperature range. To further understand static and cyclic creep deformation at moderate temperatures, it is necessary to understand these strain bursts.

It is proposed that deformation represented by these strain bursts is a result of a band of deformation moving through the material, ie a Luders Band. As discussed in the introduction of this thesis, serrated yielding is observed in standard tensile tests of Al-Mg alloys in the region of $0.4T_m$. Using photoelastic coating on tensile samples, Cetlin et al (1973) correlated the drop in load observed during serrated yielding with Luders band propagation on the sample. Many other investigators (Thomas 1966, McCormick 1974, MacEwen and Ramaswami 1967) have also reported Luders band propagation as the cause for serrations observed during serrated yielding. In addition to observations during tensile tests, Shepard and Dorn (1956) reported nucleation and propagation of several Luders bands as the reason for a single strain burst observed under constant stress in their study of delayed yielding in Al-2%Mg at 78 and 114K.

To confirm the existence of Luders bands during static and cyclic creep, several experiments were performed.

The first experiment entailed measuring axial and diametral strain coincidentally. Figure II-2 shows the experimental configuration of this test. A typical strain-time trace of one strain burst is shown in Figure III-3. The observed behavior shown in this figure is rationalized in the following paragraphs.

The total strain observed during a strain burst or Luders band cycle is made up of two components, ϵ_c , the "normal" creep strain and ϵ_L , the so called Luders strain. The total strain measured through one cycle should be independent of method of measurement. Within experimental uncertainty, this is true as shown in Figure III-3. Assuming the Luders band velocity is constant, the time period over which the intermittent Luders strain will influence the strain measured by the diametral extensometer is proportional to the length of contact between the extensometer and the sample. Since the strain increment is also constant the strain rate will also be proportional to the extensometer-sample contact length. It is clearly shown in Figure III-3 that the time during which the propagation of a Luders band affects the measured diametral strain, 120 seconds, is much less than the 435 seconds during which the Luders band affects the axial strain.

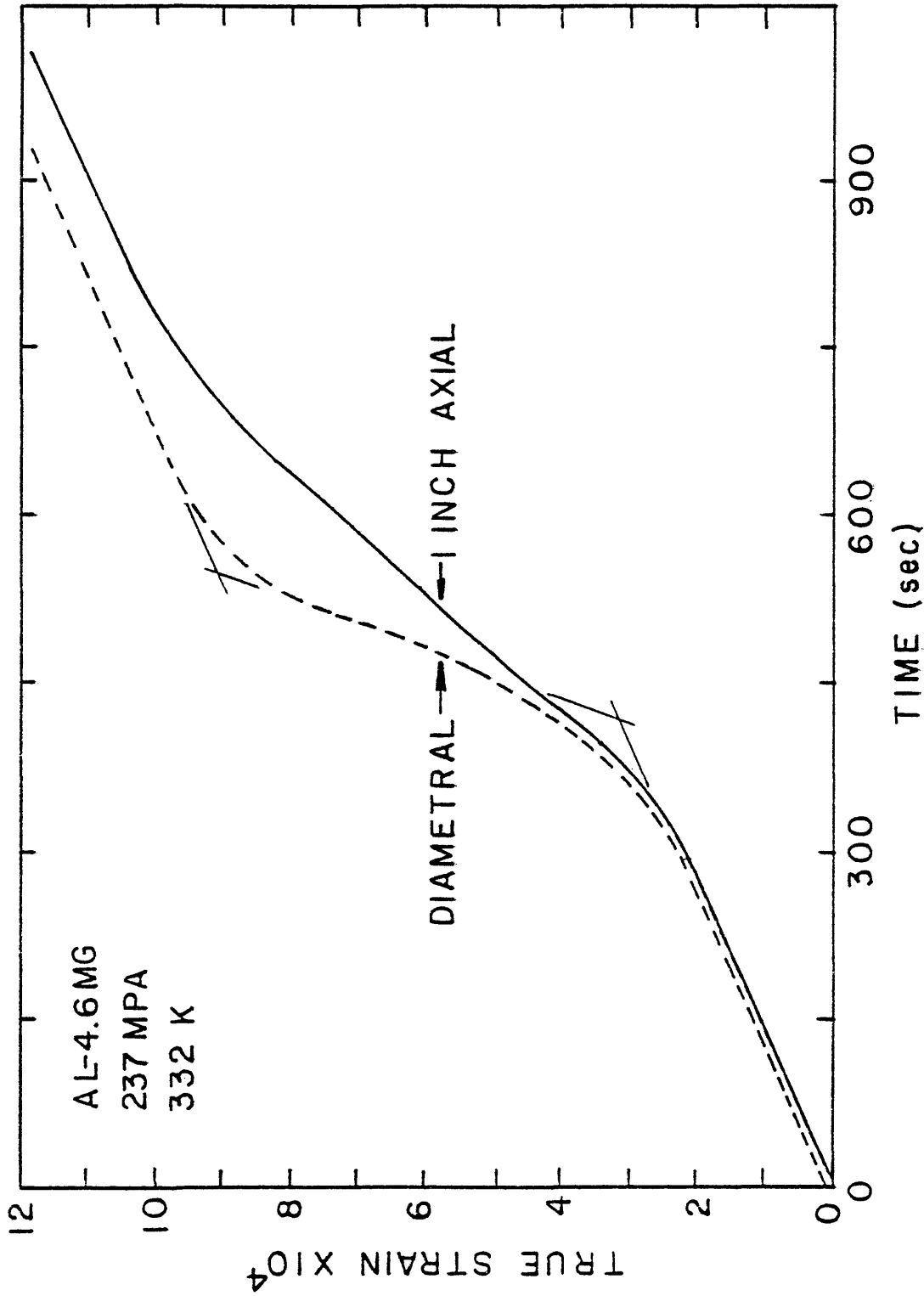


Figure III-3: Strain-time as recorded by a diametral and a 1 inch axial extensometer concurrently during "steady state" creep. Test conditions: 332K, 237 Mpa, static loading, 1 inch gauge length.

The time measurement is made by approximating the strain burst with straight lines as shown in Figure III-3.

The inflection point strain rate is also correspondingly faster in the diametral case shown in Figure III-3 as expected.

A slight modification on the dual extensometer experiment is shown in Figure III-4. During this experiment, the diametral strain was continuously recorded and initially compared to strain measured by a two inch extensometer. Later in the experiment, the two inch extensometer was replaced with a one inch extensometer. Figure III-4 shows the strain-time trace a typical strain burst as recorded by all three extensometers. As is evident, the time period for the strain burst increases with sample contact length as expected. The strain burst was observed for 90 seconds by the diametral extensometer, 250 seconds by the one inch axial extensometer, and 835 seconds for the two inch axial extensometer.

If the sample were to deform homogeneously, equivalent strain-time curves regardless of extensometer-sample length would be expected. Observations discussed above were obtained under static loading conditions. Similar experiments were also performed under cyclic loading conditions.

Figure III-5 is a direct trace of extensometer

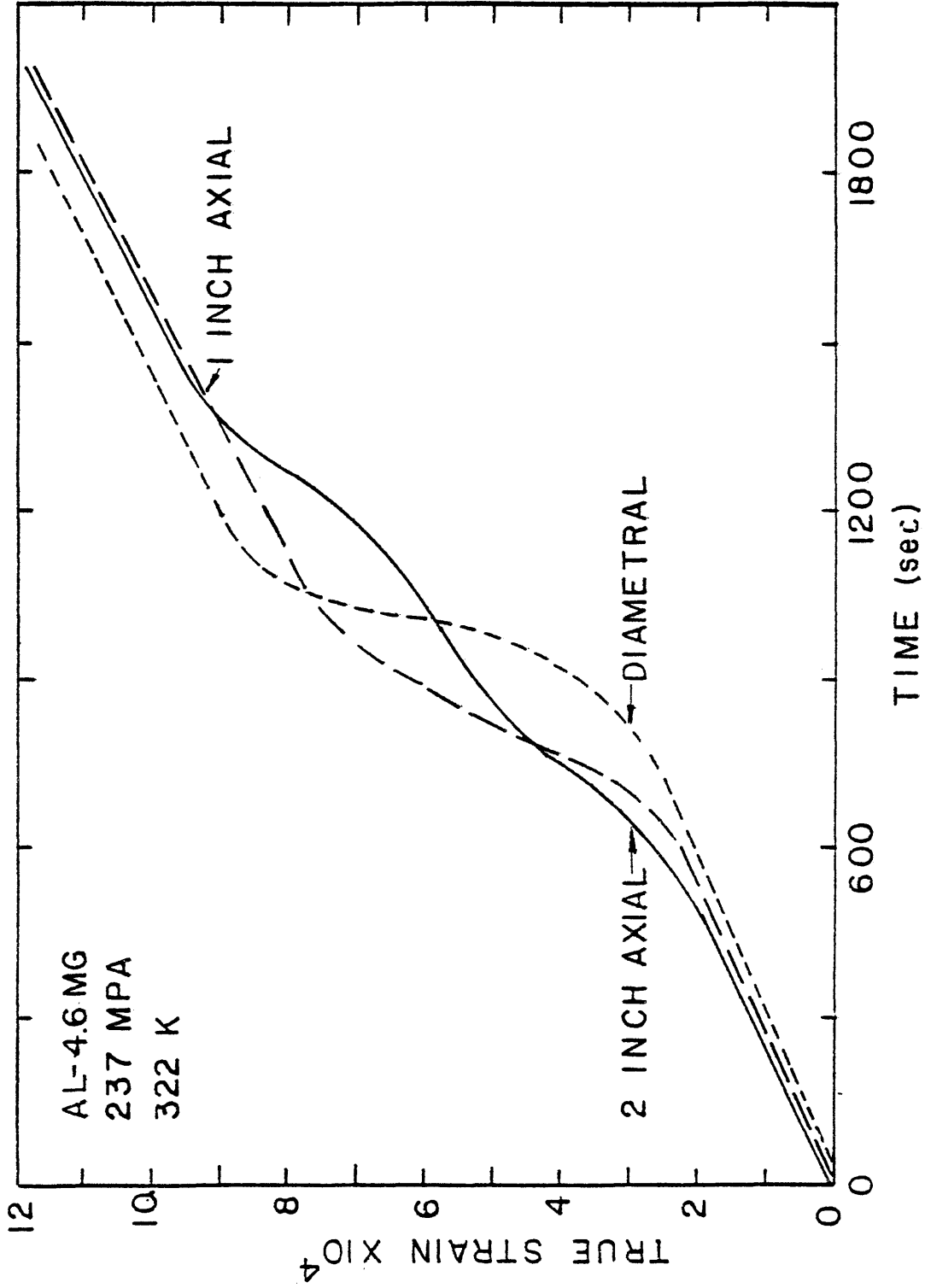


Figure III-4: Strain-time as recorded by a diametral, 1 inch axial and 2 inch axial extensometers during "steady state" creep. Test conditions: 322K, 237 Mpa, static loading, 2 inch gauge length.

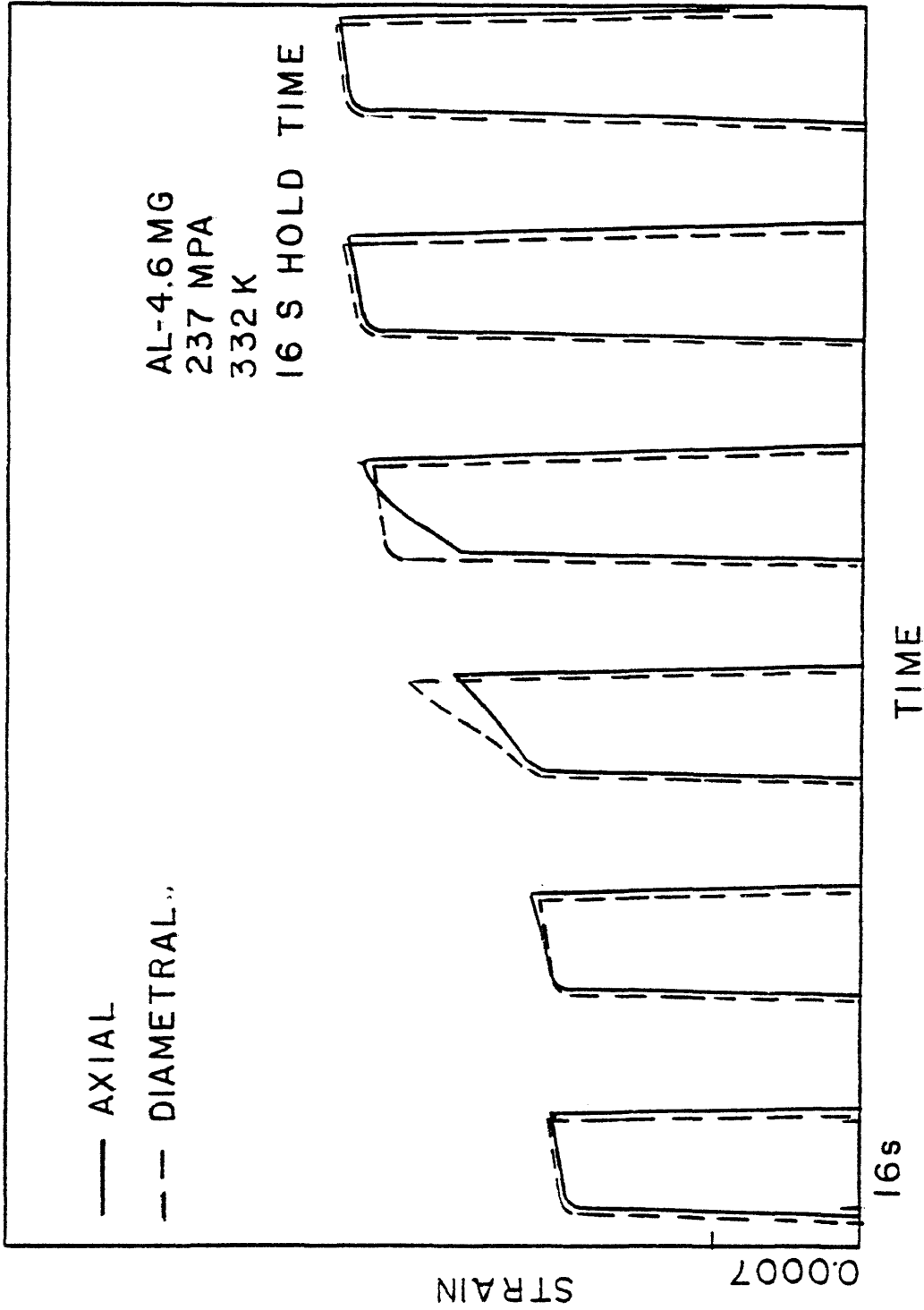


Figure III-5: A direct trace of experimental strain-time data from a cyclic dual extensometer experiment. Test conditions: 332K, 237 Mpa peak stress, 90% load amplitude, 0.027 hz loading frequency (16 s hold time), 1 inch gauge length.

332

outputs during a cyclic experiment. The delay between the end of the strain burst on the diametral trace and the end of the strain burst on the axial extensometer trace, approximately 20 seconds, is shown in this figure. This observation along with the observation of equal strain increments implies that strain bursts during cyclic creep are similar to those observed during static creep. The similarity between static and cyclic strain bursts indicates that a Luders phenomena is responsible for strain bursts in both cases.

Several other indirect observations were made that provide additional confirmation of Luders bands during static and cyclic creep. During static creep at 331K, a smooth sample was scratched with a carbide scribe. As shown in Figure III-6, a very large rapid increment of strain was recorded immediately after the sample was scratched. This large increment of strain indicates that many Luders bands were nucleated as a result of the high stress concentration caused by the scratch. Based on an average strain per Luders band of 0.0007, it is estimated that approximately 7 Luders bands propagated through the sample during this scratch test.

Shepard and Dorn (1956) observed similar results in their study of delayed yielding in Al-2%Mg. A strain-

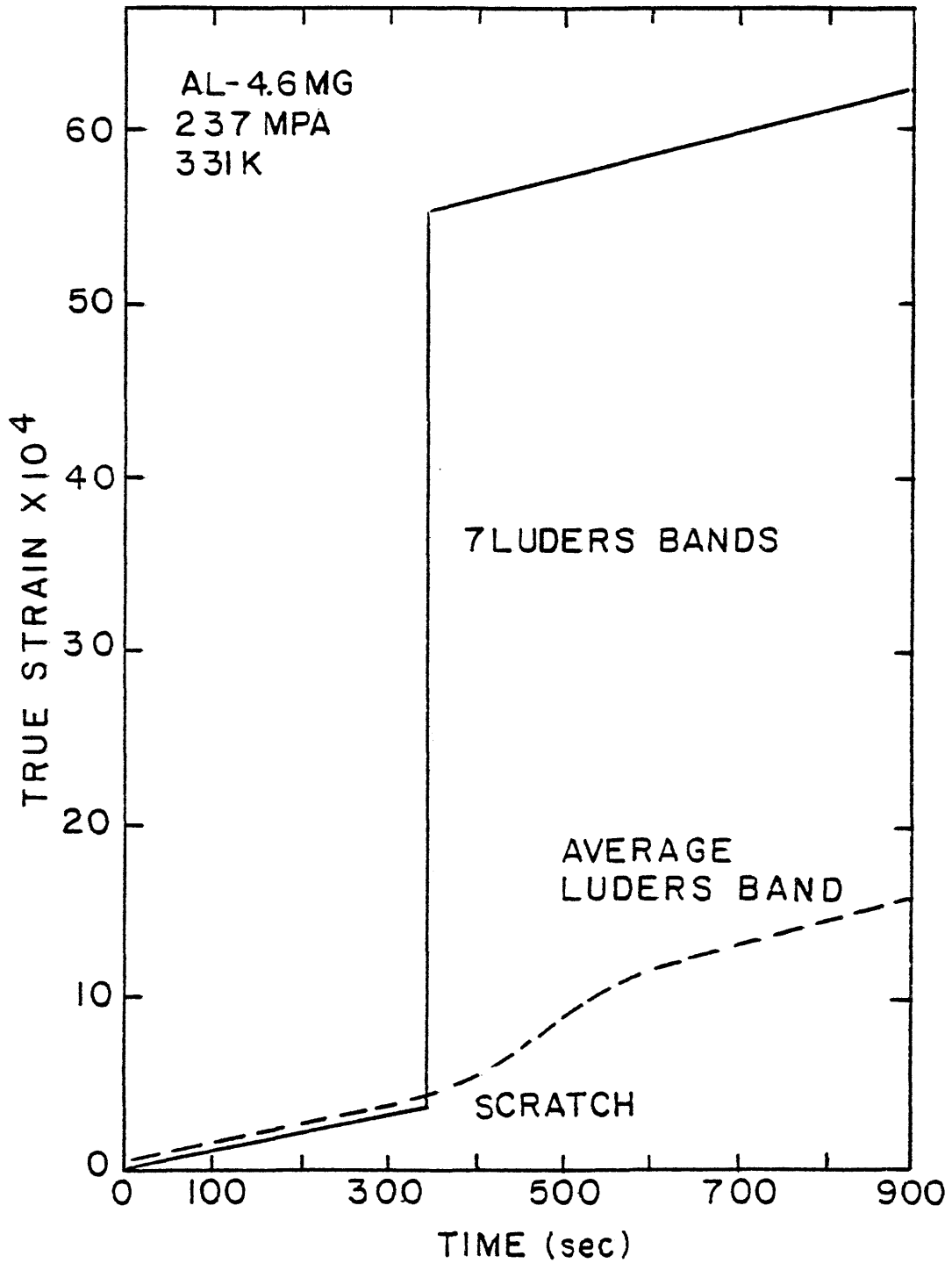


Figure III-6: Comparison of average strain burst to strain burst observed after a smooth sample was scratched. Test conditions: 331K, 237 Mpa, static loading, 1 inch gauge length.

aged sample under constant stress at 78K was indented about 60 seconds after loading, immediately nucleating a Luders band. In a similar test a 1200 second waiting time after loading was observed before nucleation of a Luders band in an unindented sample.

At 322K, several examples of Luders bands nucleating and propagating only a short distance were observed. In these cases, axial motion, as shown in Figure III-7, was observed without any change in diametral strain rate. It is theorized that the Luders band nucleated at indentations caused by the knife blades of a shorter extensometer that had been placed on the sample earlier in the experiment. This band then propagated away from the diametral extensometer toward the end of the gauge length. So long as the Luders band did not pass through the area of contact between the diametral extensometer and the sample, no strain burst would be recorded by the diametral extensometer.

Table 1 summarizes another important correlation. At a given temperature and peak stress, the average strain per Luders band, the Luders strain - ϵ_L shown on Figure III-2, is tabulated. One observes that for a constant stress and temperature, the Luders strain is essentially constant, independent of loading function. At 318K and

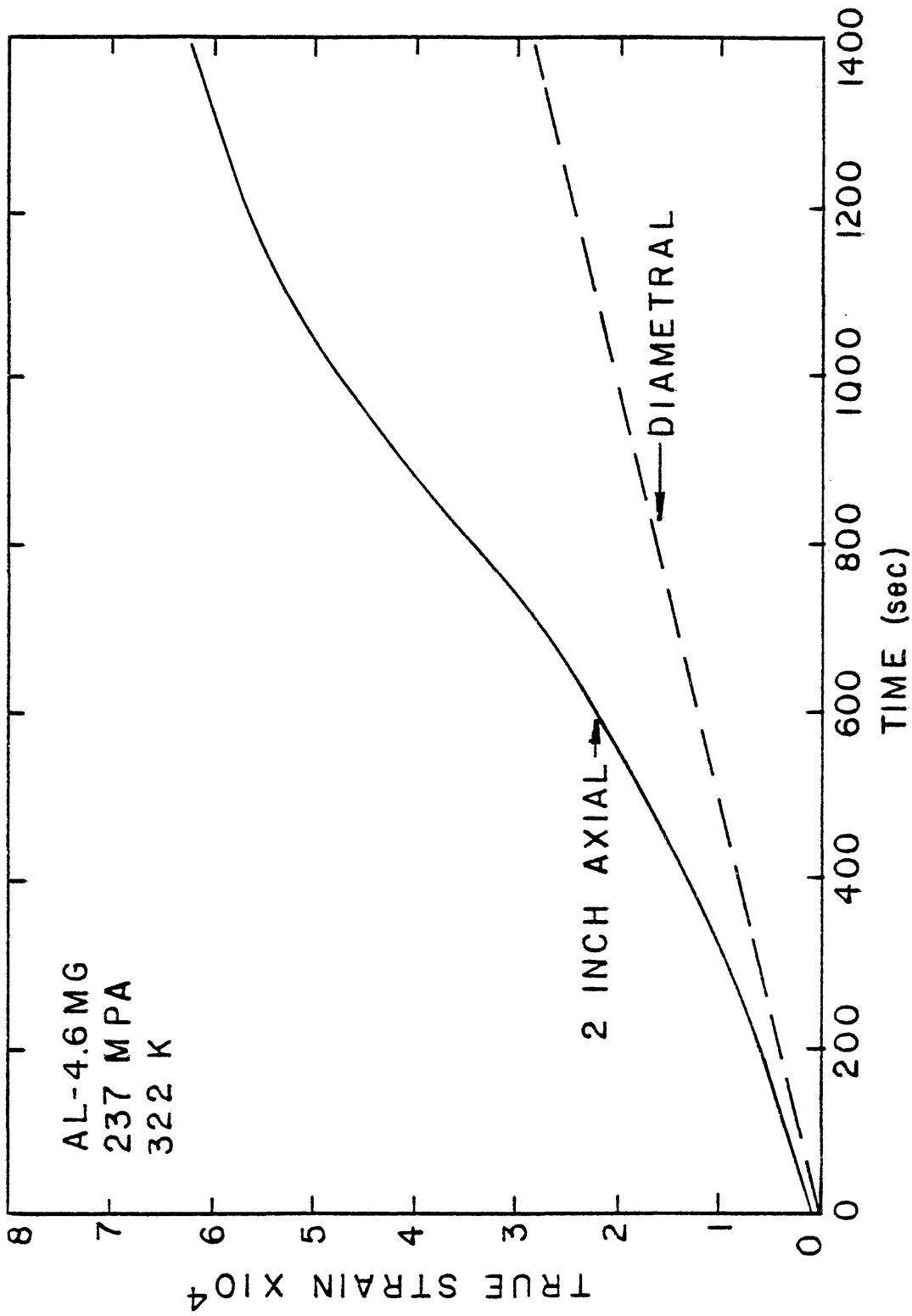


Figure III-7: Diametral and 2 inch axial extensometer strain-time trace during a "partial" propagating Luders band. Test conditions: 331K, 237 Mpa, static loading, 2 inch gauge length.

TABLE III-1

Average strain increment observed
 during strain burst at constant
 peak stress of 237 Mpa.

Temperature (K)	Test Conditions	Strain Increment
318	static	.0004
318	cyclic 16s hold time	.00036
318	cyclic 4s hold time	.00026
318	cyclic 1s hold time	.00024
328	static	.00068
328	cyclic 16s hold time	.00062
328	cyclic 4s hold time	.00065
328	cyclic 1s hold time	.00074
338	cyclic 16s hold time	.00059
338	cyclic 4s hold time	.00066
338	cyclic 1s hold time	.00064
348	cyclic 16s hold time	.00062
348	cyclic 4s hold time	.00059
348	cyclic 1s hold time	.00061
358	cyclic 16s hold time	.000838
358	cyclic 4s hold time	.000963
358	cyclic 1s hold time	.000608

237Mpa peak stress, the Luders strain averages 3.15×10^{-4} . This value increases to 6.78×10^{-4} with an increase in temperature of 10K. The consistency of Luders strain under varying loading conditions provide additional confirmation that static and cyclic strain bursts are the same phenomena.

To summarize this section, strain bursts during both static and cyclic creep are shown to result from the nucleation and propagation of Luders bands. The next section will discuss the temperature dependence of nucleation of Luders bands during creep and the corresponding importance of the Luders bands in controlling the overall creep rates.

TEMPERATURE DEPENDENCE OF LUDERS BAND

NUCLEATION DURING CREEP

As discussed in the previous section, the frequency of Luders band nucleation $1/t_t$, is a function of temperature. Specifically, the frequency decreases as the temperature decreases. The mechanism of Luders band nucleation, which controls the frequency of occurrence, is known to be a solute, diffusion related phenomena (Cottrell 1953). Assuming constant stress and structure, the frequency

of Luders band nucleation can be described by an Arrhenius rate equation of the form.

$$f=1/t_t=K\exp(-Q/RT) \quad (\text{III-1})$$

where f is the frequency of Luders band nucleation, t_t is the time between nucleation events as shown in Figure III-2, K is the rate coefficient, Q is the apparent activation energy for the process, and R and T are the gas constant and absolute temperature respectively. Based on Equation III-1, the activation energy can be obtained from the slope of the $\ln 1/t_t$ versus $1/T$ plot.

In Figure III-8, the activation energy for Luders band nucleation during static creep is determined to be 72.8 kJ/mol (17.4 kcal/mol) between 318 and 333K. Similarly, Figure III-9 yields the activation energies for nucleation of Luders bands during cyclic creep. The activation energies and frequencies are summarized in Table III-2.

TABLE III-2

Apparent activation energies for cyclic creep between 318K and 358K at three frequencies. Obtained from Figure III-9.

Frequency (Hertz)	Hold Time (sec.)	Apparent Activation Energy	
		(kJ/mol)	(kcal/mol)
0.0266	16	81.6	19.5
0.0862	4	85.0	20.3
0.132	1	76.6	18.3

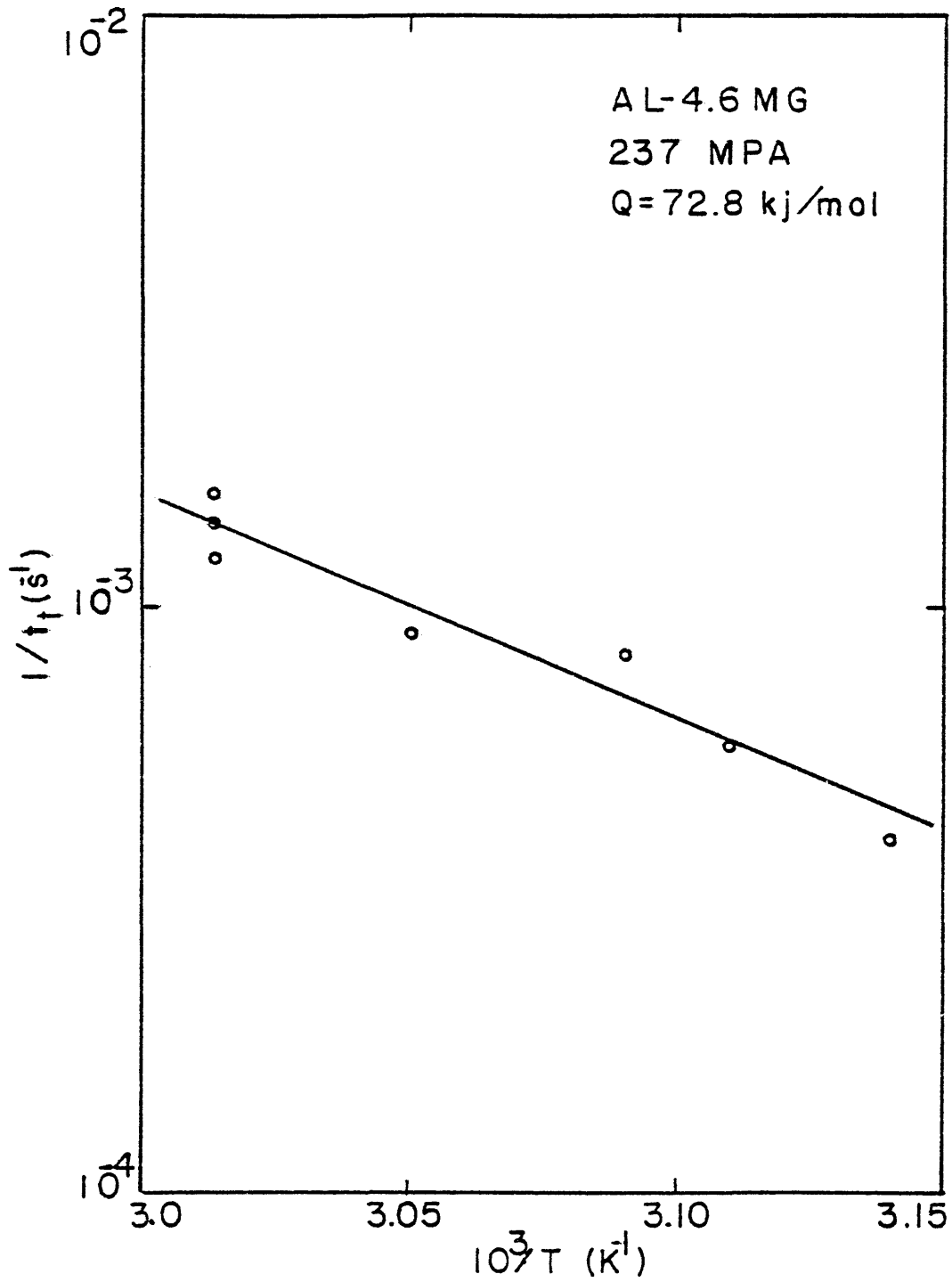


Figure III-8: Temperature dependence of the frequency of Luders band nucleation during static creep at 237 Mpa.

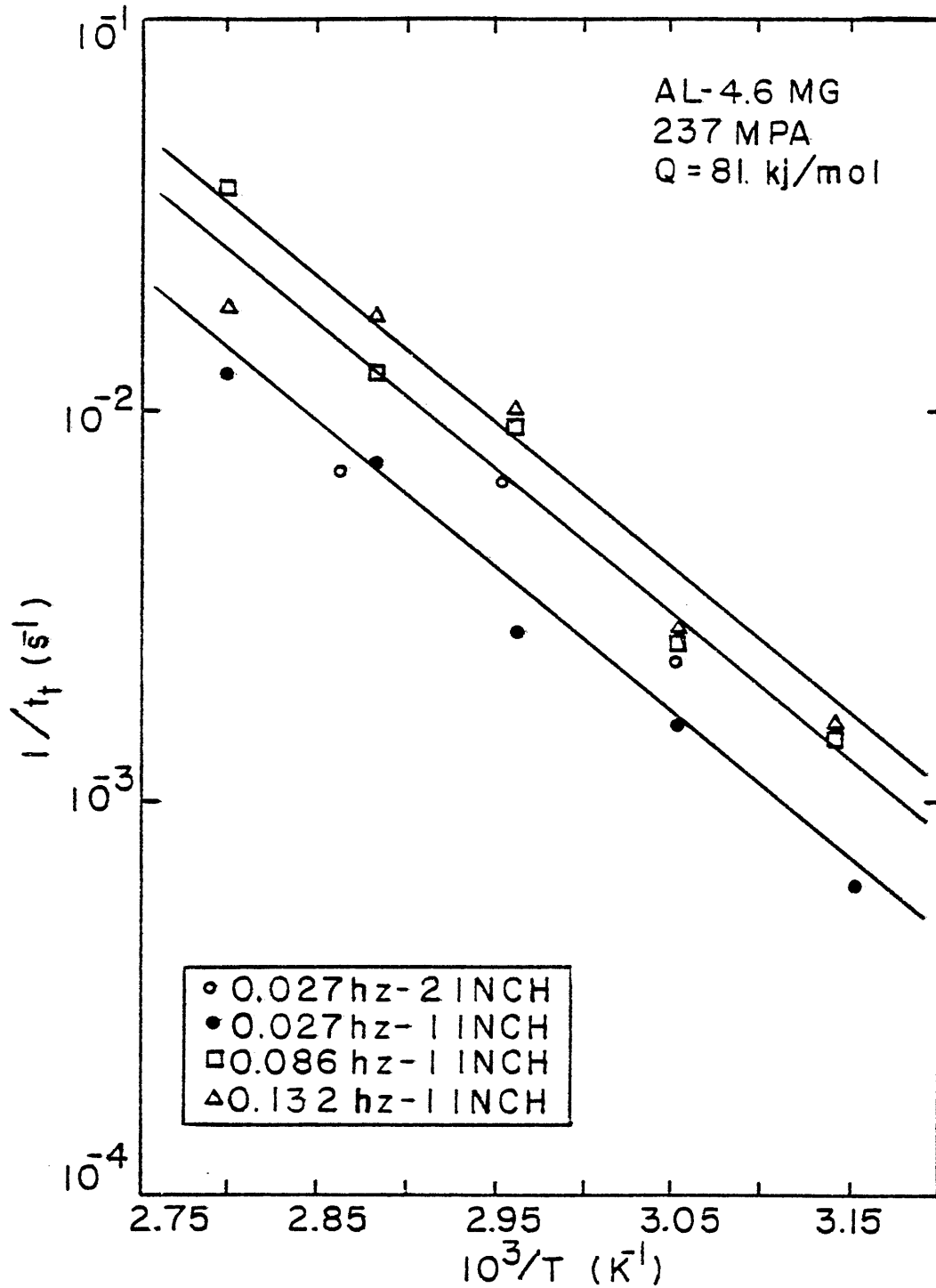


Figure III-9: Temperature dependence of the frequency of Luders band nucleation during cyclic creep at 0.027, 0.086, 0.132 Hz and a peak stress of 237 Mpa.

In the temperature range of 318 to 358K, the activation energy for the nucleation of Luders bands during cyclic creep was found to be independent of frequency and equal to approximately 81 kJ/mol (19.3 kcal/mol).

The value of total time, t_t , plotted on all Arrhenius plots is the average of several strain burst cycles, usually five or more, measured during "steady state" creep. The inherent error in the t_t measurement is fairly large, especially in the lower temperature region. For example the average time between nucleation events at 318K under static loading conditions is 2440 ± 800 seconds. The uncertainty in this case is approximately 33%. The average uncertainty for all t_t measurements is on the order of 20% for both static and cyclic experiments. While high, the uncertainty quoted is not unreasonable when one considers the phenomena under investigation. To nucleate a Luders band, a critical resistance to dislocation motion must be reached, usually at some stress concentration. Included as stress concentrators are sample fillets, machining marks, nicks, and surface irregularities, caused by non-uniform grain deformation, i.e. orange peel. Work hardening must be considered from two sources, ϵ_c and ϵ_L , along with recovery occurring

at these temperatures. The uncertainty in the time between nucleation events stems from slight variations in these variables. Cetlin et al (1973) cite the randomness of the nucleation of Luders bands in their work on serrated flow.

While error in individual data is fairly large, the average total time values do not greatly vary from each other when measurements are made during several experiments performed under identical experimental conditions. As shown in Figure III-8, at 333K, variations are slight and are within variations expected due to slight strain rate variations between different samples. (Appendix 1 contains an amplification of these strain rate variations).

The trends defined by the average total time values are definite. The critical information presented in this thesis is based on trends, not individual data.

In Figure III-10, the data shown in Figures III-8 and III-9 are combined to examine the temperature dependence of the nucleation of Luders bands during both static and cyclic creep. Two important observations should be noticed. First, the activation energies are essentially equal for both static and cyclic creep and average 74 kJ/mol (17.5 kcal/mol) and secondly, there is an increase in the strain burst frequency as loading frequency is increased.

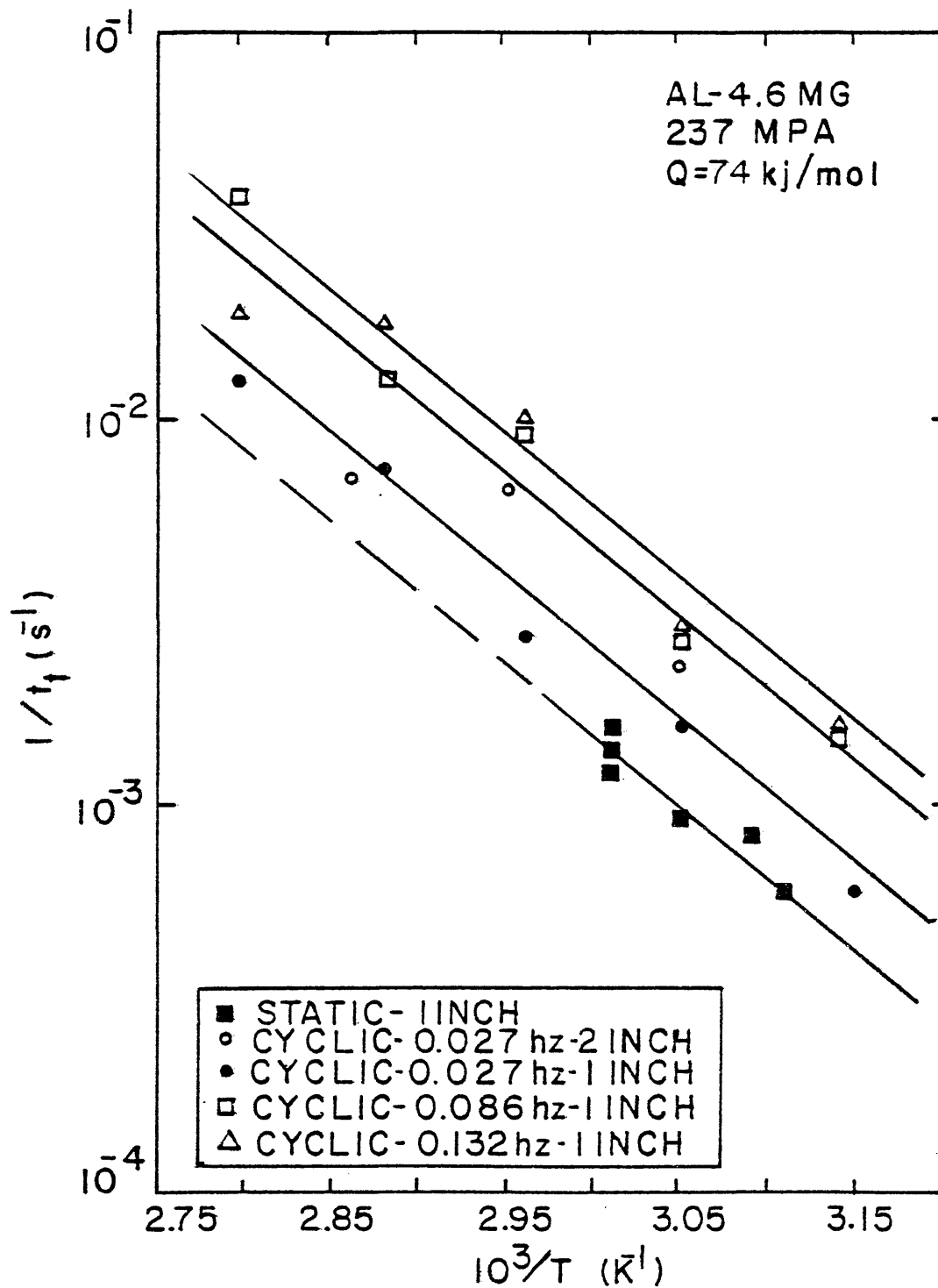


Figure III-10: A combination of Figures III-8 and III-9 showing the temperature dependence of Luders band nucleation during static and cyclic creep.

The equality of activation energies indicates that identical mechanisms control the nucleation of Luders bands during both static and cyclic creep. Furthermore, the activation energy of 74 kJ/mol compares favorably with the activation energy of 77 kJ/mol reported in the literature for nucleation of Luders bands during tensile tests of this alloy system at approximately $0.4T_m$ (Mulkherjee et al 1968). Tensile test data obtained in this investigation also compares favorably as discussed later in this chapter. These activation energies also compare favorably with the activation for vacancy migration in aluminum, 63 kJ/mol (Brindley and Worthington 1969).

The second point observed in Figure III-10 pertains to the increase in strain burst frequency with an increase in loading frequency. In Figure III-10, one can observe that the curves move progressively up as the loading frequency increases. The position of these curves relates to the rate coefficient, K , in equation III-1. The relative spacing of these curves determines the magnitude of K in each case. From this discussion, it can be determined that K , and the relative position of these curves is a function of loading frequency.

If the total strain per cycle, ϵ_t , is constant, then an increase in strain burst frequency results in an increase in average creep rate.

It can be hypothesized that one mechanism controls the nucleation of Luders bands during static and cyclic creep as well as tensile tests. A possible mechanism with the appropriate activation energy is vacancy migration. While the mechanism does not change, the rate coefficient and average creep rate is found to increase with increasing loading frequency.

ANALYSIS OF SERRATED YIELDING BY TENSILE TESTS

An analysis of serrated yielding, as observed in standard tensile tests, in Al-4.6%Mg between 293 and 358K was included in the experimental program. The purpose of these experiments was to confirm that the temperature and strain rate dependence of this alloy at these temperatures was similar to that reported in the literature.

Tensile tests were conducted at various strain rates and temperatures to confirm the literature values of the activation energy for the initial serration, Q , 77 kJ/mol, and the strain rate dependence, β -2.88 (Mukherjee et al 1968). Strain rates of 10^{-3} s^{-1} , 10^{-4} s^{-1} , and 10^{-5} s^{-1} were chosen to approximate the peak strain rate during a strain burst, the average strain rate, and the creep strain

rate observed between strain bursts respectively. Test temperatures varied from 293K to 358K. As expected, Type II serrations were observed with the possible exception of $\dot{\epsilon}=10^{-3}$ at 293K where both types of serrations were noted. Brindley and Worthington (1969) also report the transition between Type I and Type II serrations to be at room temperature for high purity Al-3%Mg. Cetlin et al (1973) observed non-propagating Luders bands to be characteristic of Type II serrations. This is contrary to the observation during cyclic creep of predominately propagating Luders bands. This difference is thought to result from the difference in test techniques, creep tests at approximately constant stress and tensile tests at constantly increasing stress. Further investigation of the differences was not undertaken.

As reviewed in the introduction, the slope of the $\ln \epsilon_s$ versus $1/T$ plot, Figure III-11, yielded an activation energy for the initial serration of 75.3 kJ/mol (181 kcal/mol) using a β value of -2.88 per Mukherjee et al (1968). This activation energy compares favorably with 77 kJ/mol observed by Mukherjee et al. Accurate determination of the strain rate dependence, β , was not possible due to excessive scatter in the low strain rate data. However, the negative trend to the strain rate data with increasing temperature was observed consistent with the literature.

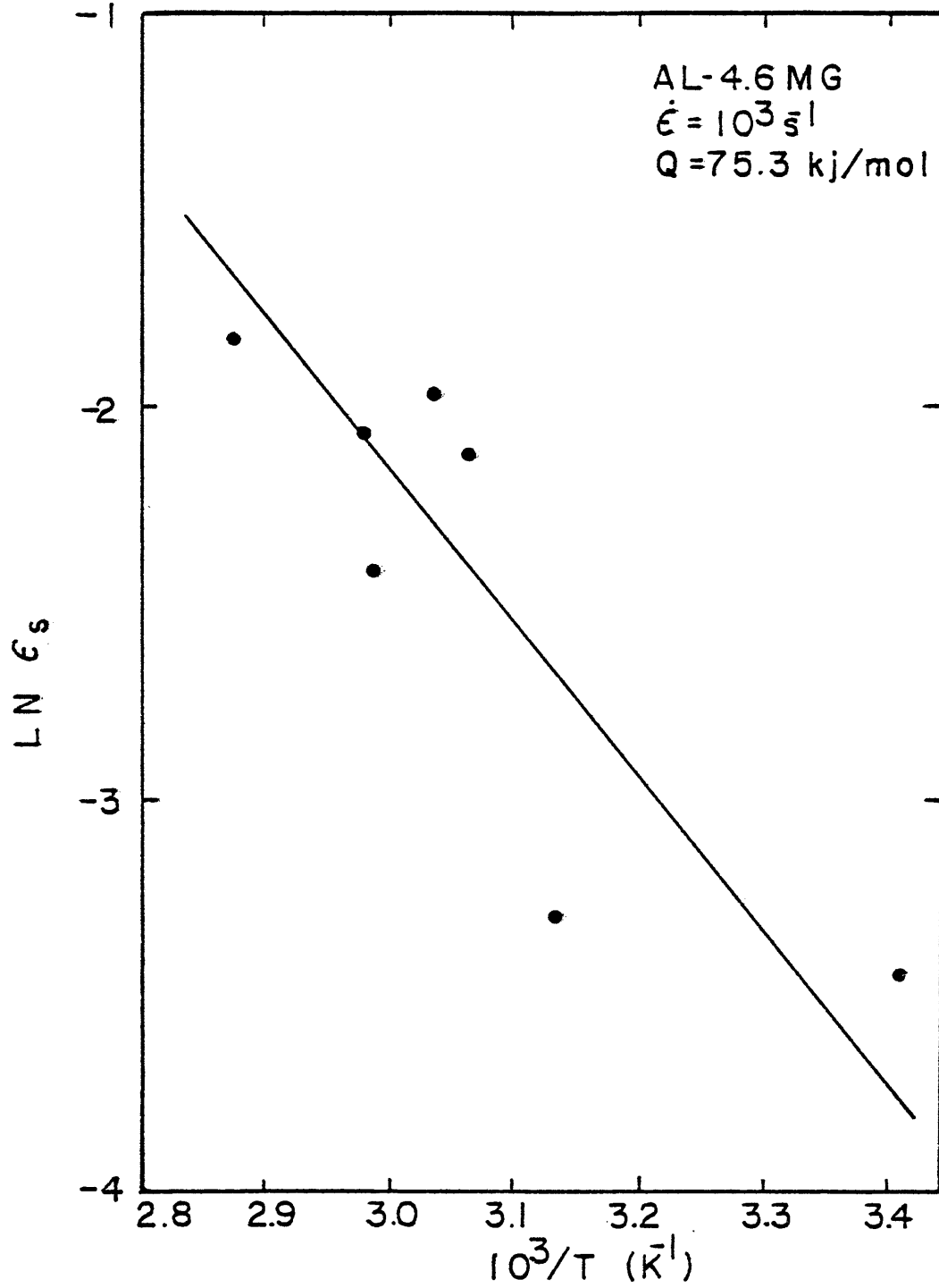


Figure III-11: Temperature dependence of the initiation of Luders bands during tensile tests.

Errors in tensile test results stem from the inability to accurately determine the strain at which the initial serration occurs. Small, irregular initial serrations and electrical noise in the measuring circuits made this determination very difficult, especially at slow strain rates.

The temperature dependence of serrated yielding, 75.3 kJ/mol, was found to be very similar to the activation energy of the initial serration reported in the literature of 77 kJ/mol. Furthermore, the activation energy observed for serrated yielding is essentially equal to the activation energy observed for nucleation of Luders bands during static and cyclic creep. The strain rate dependence, while not determined, exhibited the negative slope reported in the literature for this temperature range and alloy system.

ANALYSIS OF AVERAGE CREEP RATES

Average overall static and cyclic creep rates were determined for all experiments. The average creep rate was determined simply by dividing the total strain per cycle, ϵ_t , by the total time between nucleation events, t_t , as shown in Figure III-2. The creep rate measured

by this method averages the affect of strain bursts.

The creep phenomena is commonly described by the following expression:

$$\dot{\epsilon} = K\sigma^n \exp(-Q_c/RT) \quad (\text{III-2})$$

where $\dot{\epsilon}$ is the creep rate, K is a constant, σ is the applied stress, n is the stress dependence and Q_c is the activation energy for creep. Assuming that both static and cyclic creep can be described by this expression, their respective activation energies can be determined from the slope of the $\ln \dot{\epsilon}$ versus $1/T$ Arrhenius plot, holding stress, in the case of cyclic creep peak stress, and structure constant.

Figure III-12 is the Arrhenius plot for static creep rates. All data shown are minimum creep rates. In the temperature range of 328K to 358K, the activation energy for static creep is observed to be 123 kJ/mol (29.3 kcal/mol). Coutinho et al (1975) reported activation energies of 133-152 kJ/mol between 328K to 348K using temperature change techniques on Al-4.6%Mg. In further work on this alloy with temperature change experiments, Rising (1977), similar to the results obtained by Borch, Shepard, and Dorn (1960), showed an increasing activation energy for creep as temperature decreases. These results are summarized in Figure I-2.

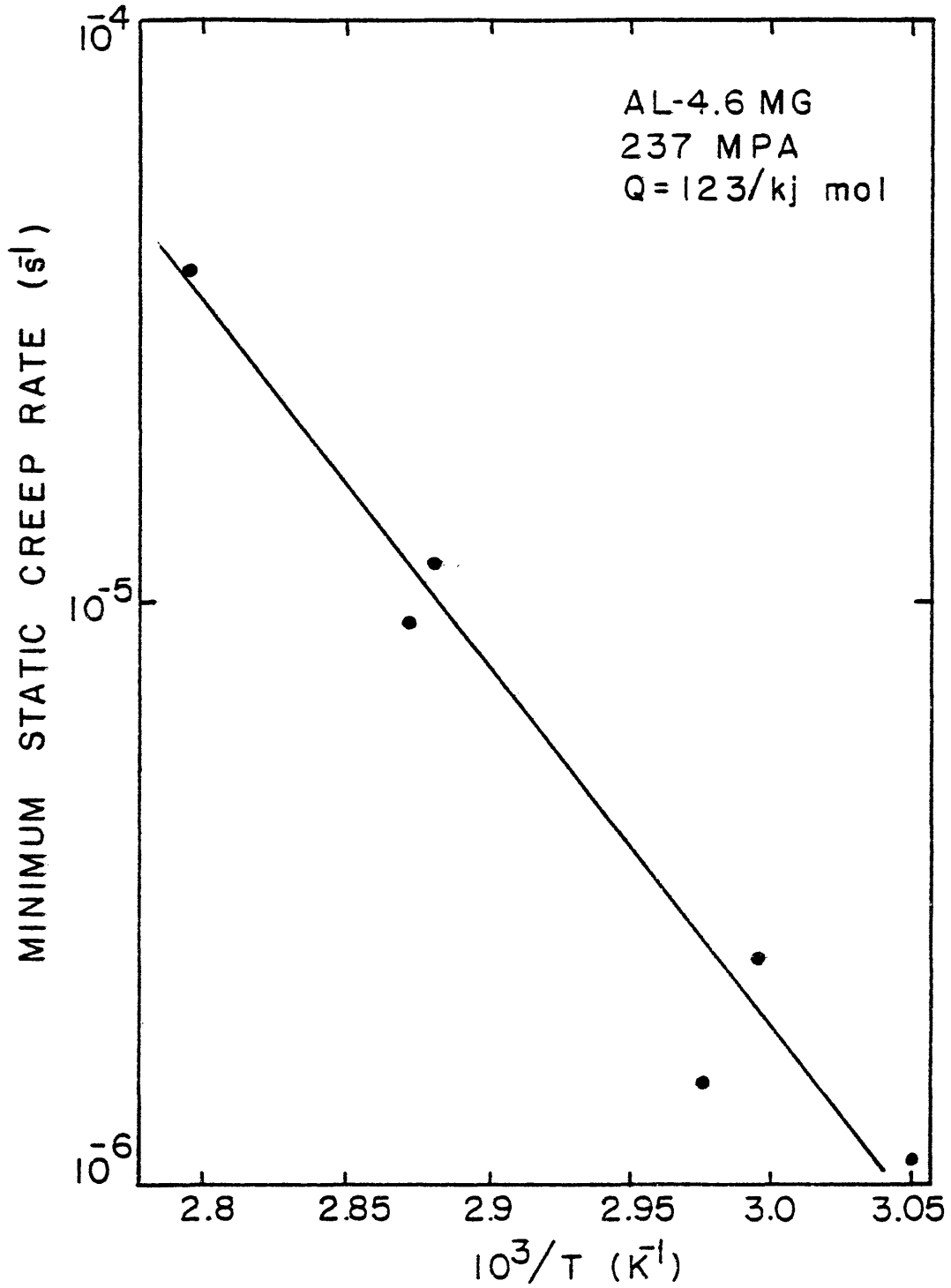


Figure III-12: Temperature dependence of minimum static creep rates tested at a stress of 237 Mpa.

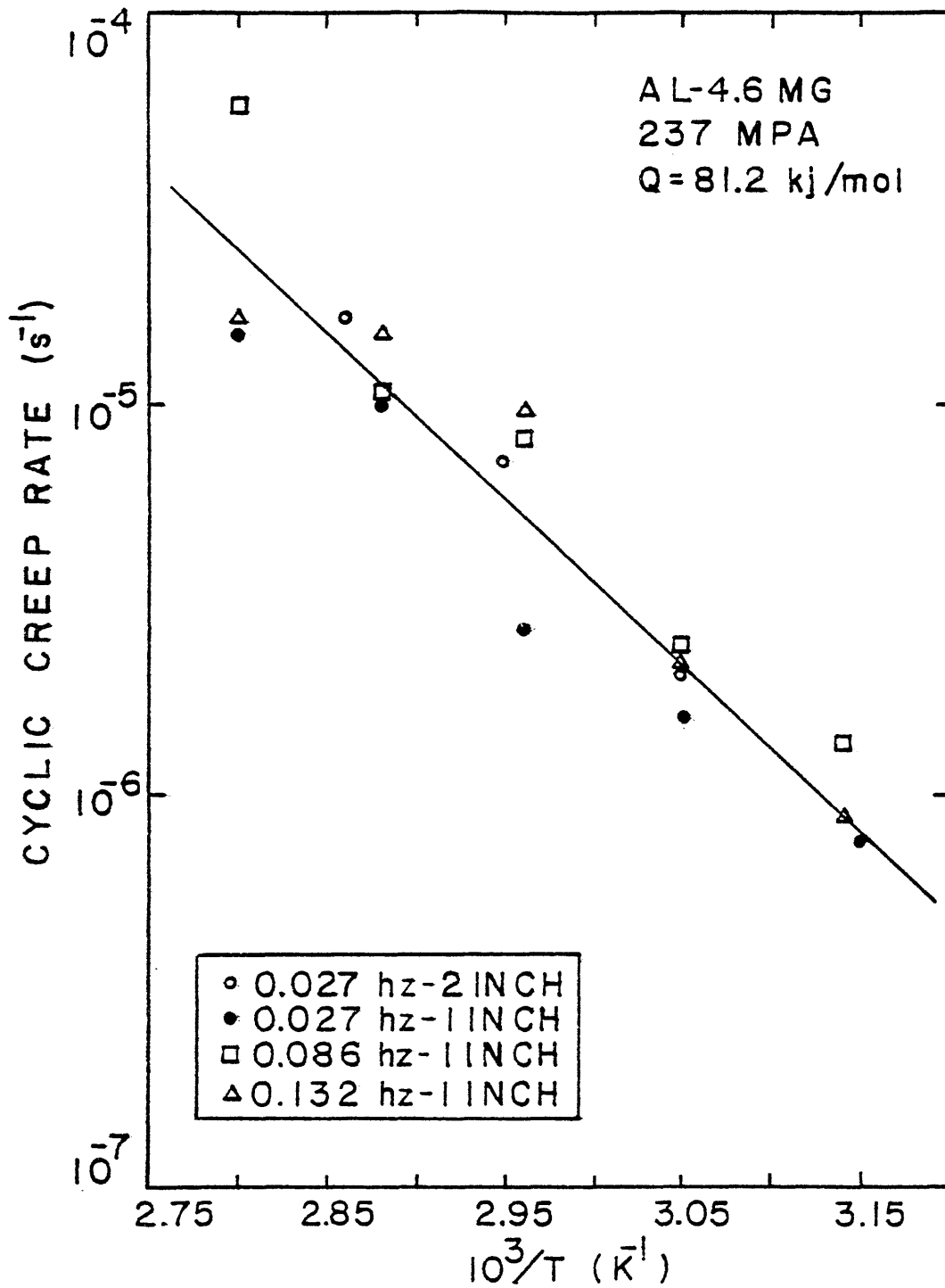


Figure III-13: Temperature dependence of cyclic creep rates observed during mode change tests at a peak stress of 237 Mpa, 90% load amplitude and three loading frequencies.

The activation energy for static creep observed in this thesis does not show the increasing trend shown in Figure II-2. Activation energies shown in Figure II-2 were obtained using temperature change techniques. This technique involves measuring the creep immediately before and after a slight change in temperature. The activation energy is thus measured over a very short period of strain. The measured activation energy could vary greatly depending on whether it was measured during a strain burst, or during the period of "normal" strain rate between strain bursts. The scatter of activation energy values measured in this temperature range is large as discussed in the work of Borch, Shepard, and Dorn.

The technique used in this thesis for creep activation energy measurements averages the strain rate over both the "normal" strain rate portion of the creep curve and the strain burst portion. The average effect of this technique, at least in the temperature range investigated, does not allow the activation energy peak to be observed.

The activation energy for cyclic creep was determined by an average creep rate method. As shown in Figure III-13, the observed activation energy for cyclic creep is 81.2 kJ/mol (19.4 kcal/mol) in the temperature range between 318K and 358K. The cyclic strain rate data used in this

figure was obtained from mode change tests. The strain rates plotted closely approximate the minimum strain rate values. Since minimum strain rate has been shown to be independent of frequency in Al-4.6%Mg under similar conditions, only one curve is drawn in Figure III-13.

Limited literature comparisons are available for cyclic creep activation energies. Coutinho et al (1975) reported considerably higher activation energies for cyclic creep than observed in this work. 140 kJ/mol was the average activation energy between 324K and 353K reported in Coutinho's work. Rising (1977) reported somewhat lower activation energies than Coutinho as shown in Figure II-2. Below 375K, Rising also reported cyclic creep activation energies systematically lower than static creep activation energies.

As stated in the introduction, the basic purpose of this thesis is to study cyclic creep acceleration. Table III-3 summarizes static and cyclic creep rates observed during mode change experiments. The static creep rates tabulated are measured immediately before the mode change. Cyclic creep rates tabulated are measured after the transient into the "steady-state" portion of cyclic creep. As can be observed in Table III-3, the

TABLE III-3

Summary of static and cyclic
 creep rates from mode change test at 237 Mpa peak
 stress under various condition.

Temperature (K)	Hold Time (sec)	Frequency (Hertz)	Strain Rate $\times 10^6$ (s^{-1})	
			static	cyclic
318	16	0.027	.78	.78
318	4	0.086	1.34	1.45
328	16	0.027	.79	1.56
328	4	0.086	1.65	2.4
338	16	0.027	2.5	2.6
338	16*	0.086	6.7	7.12
338	1	0.132	9.4	9.4
348	16	0.027	7.5	10.3
348	16*	0.027	9.45	16.6
358	16	0.027	11	15
358	4	0.086	53.3	57
358	1	0.132	12	16

* 2 inch gauge length samples

static creep rate is less than or equal to the cyclic creep rate in all cases. Since static creep rates, especially at lower temperatures, may not be the minimum creep rates, cyclic creep acceleration is indicated in all cases.

Slight variations in both static and cyclic creep rates in experiments conducted under identical nominal conditions stem from three sources: (1) slight variations in nominal experimental conditions, particularly temperature and stress, (2) strain rate measurements made at different values of creep strain, and (3) inherent differences in samples. The second point is particularly important. The possibility that static strain rate measurements were made during primary creep is great, especially at low temperatures. In that case, because the minimum strain rate was not reached, the strain rate values quoted would be artificially high. Therefore, Table III-3 represents a conservative estimate of cyclic acceleration.

Inherent sample differences were observed during testing, causing random scattering of data. A summary of this subject is contained in Appendix I.

Experimental results will be further discussed and analyzed and an explanation for cyclic creep acceleration of Al-4.6%Mg at $0.4T_m$ proposed in the following chapter.

CHAPTER IV

DISCUSSION

The principles discussed in the introduction and the results presented in the previous chapter will be combined in this chapter to propose an explanation for cyclic creep acceleration of Al-4.6%Mg in the temperature range of $0.37T_m$ to $0.42T_m$. This explanation will be based on the nucleation and propagation of Luders bands during deformation at these temperatures and the effects of cyclic loading on the Luders bands.

As presented in the previous chapter, the activation energies for the nucleation of Luders bands during static and cyclic creep are essentially equal. This value of 74 kJ/mol (17.5 kcal/mol) is also essentially equal to the activation energy for the onset of Luders bands which cause serrated yielding during tensile tests. The equality of these activation energies indicates that during static creep, cyclic creep, and tensile tests the same basic mechanisms control the nucleation and propagation of Luders bands.

While the temperature dependence of the nucleation of Luders bands during static and cyclic creep is equal,

the frequency of occurrence of these strain bursts is not the same. As presented in Chapter III, the frequency of Luders bands is characteristically faster during cyclic creep as compared to static creep under similar stress and temperature conditions. This observation leads one to the conclusion that cyclic loading during creep increases the frequency of the Luders phenomena which increases the average creep rate. This results in an increased cyclic creep rate as compared to static creep, ie cyclic creep acceleration.

To understand more fully the explanation of cyclic creep acceleration, consider the conditions necessary for the nucleation of a Luders band during creep. The resistance to dislocation motion in Al-4.6%Mg in the dynamic strain aging temperature range results from two components. First there is resistance to motion due to substructural considerations such as subgrain boundaries and dislocation pile-ups. Secondly, additional resistance results from the drag of solute atmospheres surrounding dislocations.

As shown in Figure III-2, the total strain observed during creep of Al-4.6%Mg in the temperature range of interest is made up of two components, the strain occurring during strain bursts, ϵ_L , and the "normal" creep strain

which occurs between strain bursts, ϵ_c .

The following discussion will correlate the factors that control dislocation motion as mentioned in the previous paragraph to the two distinctly different portions of the deformation cycle shown in Figure III-2.

To understand the requirements for Luders band nucleation, one must consider the substructural variations that occur in a sample during the deformation cycle. This can best be done by focusing attention on one point of the sample and considering substructural changes which occur at this point during one complete deformation cycle. One must remember that the inhomogeneous deformation represented by the strain bursts causes a gradient in hardness throughout the sample.

Assume the point of interest is initially deforming in the "normal" creep portion of the strain-time curve between strain bursts. If one assumes that the solute diffusivity is high enough to quickly form saturated atmospheres, the resistance to dislocation motion due to these solute atmospheres will be constant so long as the atmospheres are intact. However, the resistance due to substructural considerations will decrease with time due to recovery of the work hardened structure caused

by previous Luders band propagation. At some point a Luders band, nucleated elsewhere, will propagate through the point of interest. The initial increase in the diametral strain rate shown on Figure III-3 would correspond to this point. Slowly moving solute "pinned" dislocations will break away from their solute atmospheres and rapidly move through the matrix. This extensive, localized deformation accompanying the Luders band will cause rapid strainhardening. The rapidly moving dislocations are slowed as a result of this Luders strain hardening. The reduced dislocation motion allows reformation of the solute atmospheres. The diametral strain rate decrease shown in Figure III-3, correspond to the point where the Luders band propagates out of the contact region between the extensometer and the sample. Recovery of the Luders strain hardening will begin softening the structure after the Luders band has passed. With understanding of the substructural variations occurring in the sample, now consider the conditions necessary for nucleation of a Luders band.

The substructural softening, discussed in the previous paragraph, will decrease the resistance to dislocation motion with time. As the resistance decreases, a critical

value will be reached, usually at a stress concentrator, where solute "pinned" dislocations in one grain move fast enough to breakaway from their atmospheres. This motion causes stress concentrations to be formed in adjacent grains that allow additional dislocations to breakaway and rapidly propagate. In this way a Luders band nucleates.

This inhomogeneous deformation results in a constantly changing gradient of hardness throughout the sample. At any instant, the sample region just ahead of the Luders band will be relatively soft and the region just behind the Luders band is work hardened due to the extensive localized deformation accompanying a Luders band.

Based on the above discussion, the frequency of Luders band nucleation is a function of two major factors, (1) the magnitude of stress concentrations, and (2) the recovery rate of the rapidly work hardened structure produced by the propagation of a Luders band. Since fillet radii and machining techniques were identical for all samples tested, it can be assumed of stress concentrations, while causing some experimental scatter, are approximately constant. This fact leaves only a variation in recovery rate of the Luders strain hardening to explain the differences

observed in Luders band frequency. Furthermore, in order to explain the faster Luders band frequency observed during cyclic creep, the recovery rate of the structure left by Luders band propagation must be faster in the case of cyclic creep as compared to the recovery rate during static creep.

Recovery is a complicated process that decreases the strength of a material by substructural softening. There are many mechanisms of recovery including annihilation of dislocations by climb and thermally activated cross slip of dislocation, from a work hardened slip plane to a less work hardened slip plane. Many of these recovery mechanisms are diffusion controlled. The following arguments assume that diffusion is the rate controlling mechanism for recovery.

Two explanations based on diffusion controlled recovery are presented to explain the increased rate of recovery during cyclic creep. Consider Fick's first law as it relates to diffusion

$$J=Cv \quad (IV-1)$$

that is the flux of atoms, J , across some plane is equal to the concentration of atoms, C , multiplied by the velocity, v , of these atoms. The velocity can be described as

$$v=MF \quad (IV-2)$$

where M is the atomic mobility and F is the driving force to move these atoms. Combining equations IV-1 and IV-2, one obtains

$$J = CMF \quad (IV-3)$$

The first explanation for increased recovery due to the Luders strain hardening during cyclic creep relates to the mobility term in Ficks first law. The Einstein-Nerst equation

$$M = D/KT \quad (IV-4)$$

relates the atomic mobility to the diffusivity. As reviewed in the introduction, plastic deformation can form excess vacancies which enhance the diffusivity. It is proposed that cyclic deformation forms a greater concentration of excess vacancies than static deformation. This results in a faster diffusivity and correspondingly faster rate of recovery from the work hardening caused by the Luders strain. Kennedy (1956) suggested a similar mechanism for cyclic creep acceleration in lead at 305K.

Coutinho (1973) calculated a relaxation time, τ , for the annihilation of non-equilibrium vacancies at sinks. At 338K this relaxation time is on the order of 60 seconds. This relatively short life time of non-equilibrium vacancies indicates their effect is only important for a relatively short time period after generation. Assuming generation

during unloading and loading, the enhanced diffusivity due to these non-equilibrium vacancies occurs only for the first 60 seconds after loading or unloading takes place.

The second explanation for the increased recovery of Luders strainhardening during cyclic creep involves the driving force term in Equation IV-3. McLean (1966) suggests that recovery is a function of internal stress raised to a power. Matlock and Bradley (1976) propose that this simple relationship does not completely characterize recovery during cyclic creep. Based on experimental observations, they suggest that recovery also depends on a microstructural instability factor. This factor is defined as the difference between the instantaneous internal stress in the material and the equilibrium internal stress that would occur in the material if it were held at the particular conditions for an infinite period of time. The microstructural instability factor is clarified in Figure IV-1 which is a stress cycle showing applied stress, instantaneous and equilibrium internal stress, and the corresponding strain cycle. The internal stress transients shown in Figure IV-1 represent a generalized case. In actuality, internal stress levels and recovery rates will vary because of the

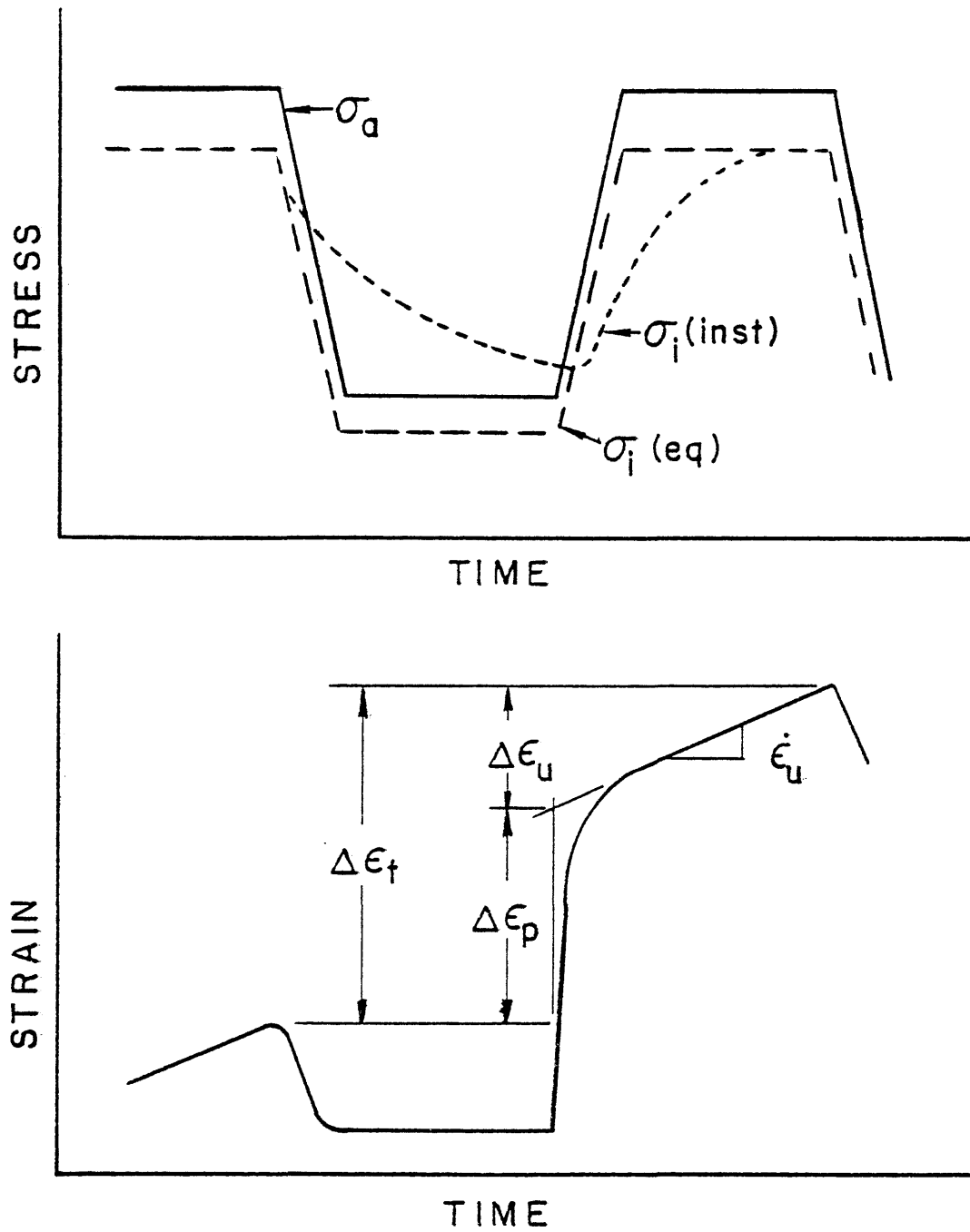


Figure IV-1: A schematic of stress and the resulting strain cycle observed during cyclic creep. Included is the proposed internal stress transients.

inhomogeneous nature of deformation observed in this work. The basic approach, however, of internal stress transients will be applicable.

Matlock and Bradley propose that the microstructural instability factor is an additional driving force for recovery, in this case recovery of the Luders strain hardening during creep.

To help understand the enhanced recovery rates during cyclic creep, consider the factors effecting recovery at several points in the load cycle shown in Figure IV-1. Immediately after unloading, the atomic mobility is enhanced due to excess vacancies that have been formed during the reverse plastic flow associated with unloading, enhancing the diffusivity. The reverse strain observed during unloading cannot completely be explained by elastic contraction. In fact, approximately half the reverse strain is elastic contraction and the rest is reverse plastic flow. The driving force is also increased due to a large microstructural instability factor and a fairly high internal stress. These factors also tend to enhance recovery. Just before reloading, the driving force is lowered due to decay of the instantaneous internal stress and the atomic mobility is decreased because of vacancy annihilation which results in slower

recovery rates. From these arguments, it is evident that recovery rates observed during cyclic creep will be faster than those observed during static creep. Because of the enhanced recovery rate during cyclic creep, the resistance to dislocation motion caused by the work hardening associated with Luders band propagation will decrease faster than during static creep. Since the resistance to motion decays faster during cyclic creep, the frequency of Luders band nucleation will increase. The additional Luders strain resulting from the increased nucleation frequency causes cyclic creep acceleration.

The explanation presented above will now be correlated with cyclic acceleration work performed by several previous investigators. In these previous investigations, two distinct modes of cyclic creep acceleration have been observed. $\Delta \epsilon_p$ control, which is characterized by large instantaneous strain increments upon reloading and slow upper stress strain rates similar to the static strain rate. This mode of acceleration was observed in Al-4.6%Mg by Knaus (1975) and is shown in Figure IV-2. $\dot{\epsilon}$ upper control observed by August (1977) in high-purity aluminum, is characterized by small strains upon reloading and upper stress strain rate considerably faster than the

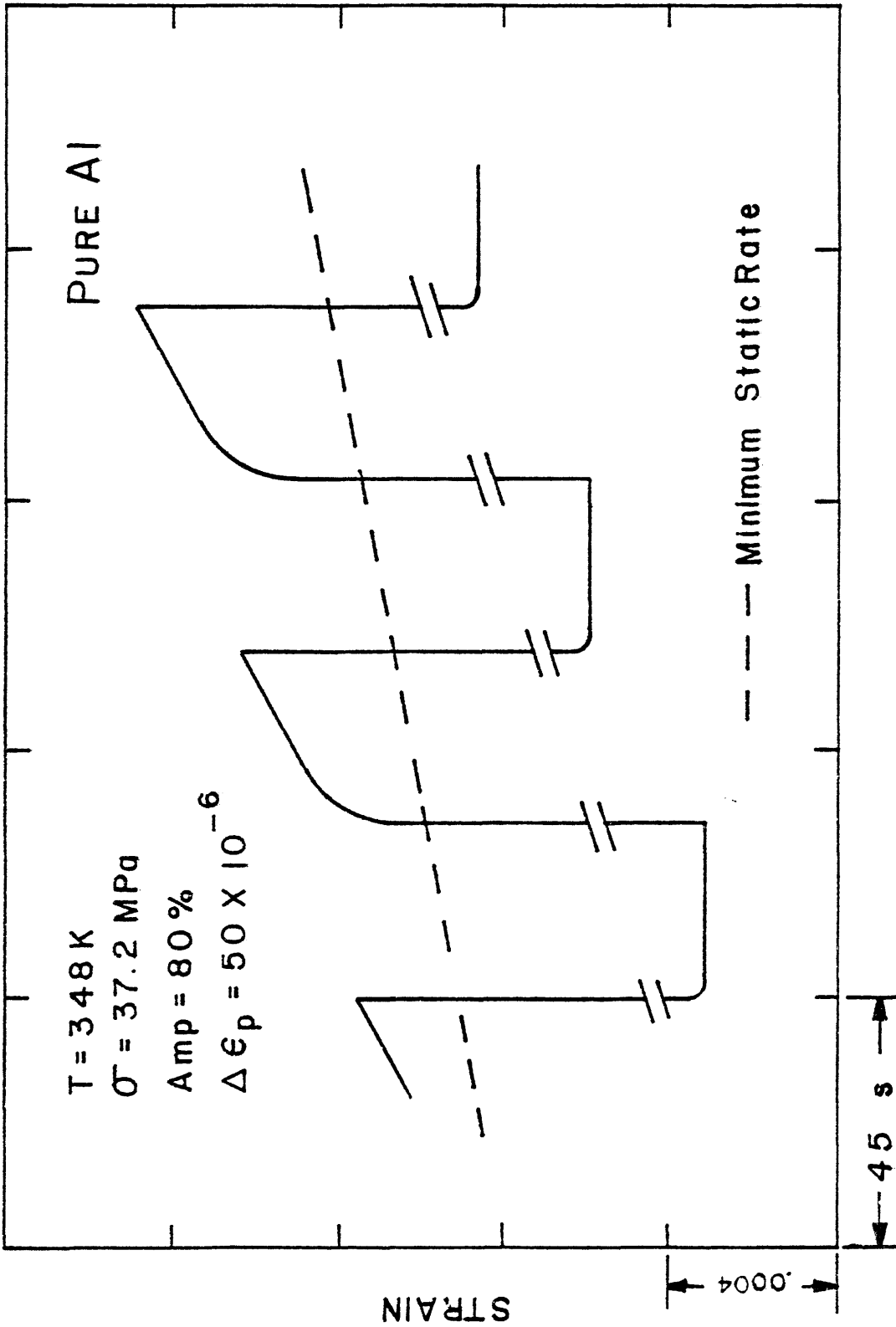


Figure IV-2: Strain-time data showing $\dot{\epsilon}$ upper controlled cyclic creep acceleration in high-purity aluminum. Test conditions: 348K, 37.2 Mpa, peak stress, 80% loading amplitude, 0.017 hz.

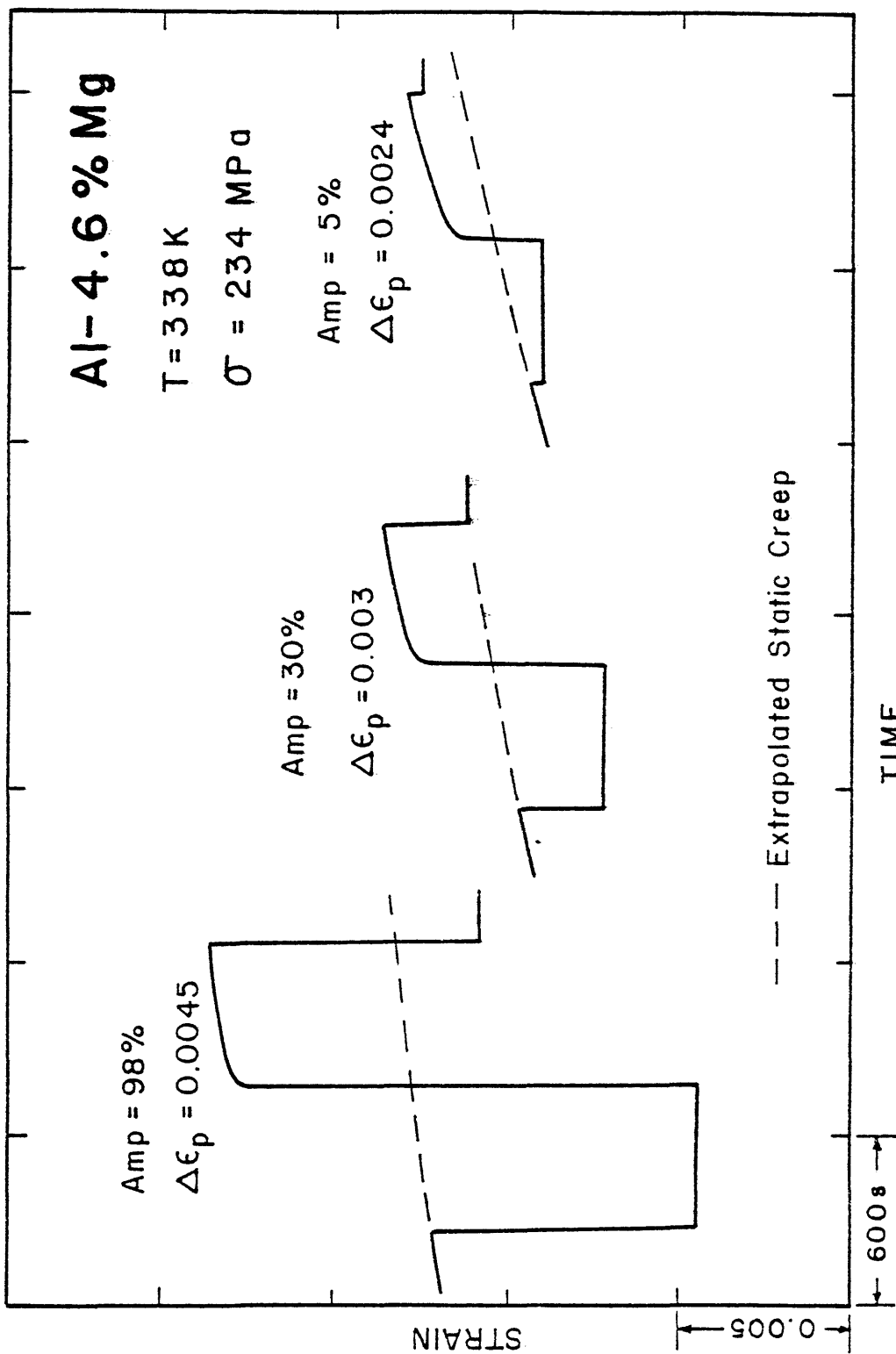


Figure IV-3: A direct trace of strain-time data showing $\Delta\epsilon$ controlled cyclic creep acceleration in Al-4.6%Mg. Test conditions: 338K, 237 Mpa peak stress, 0.001 hz (500 s hold time), and three amplitudes.

static strain rate. $\dot{\epsilon}$ upper controlled acceleration is shown in Figure IV-3.

It is hypothesized that the characteristics of $\Delta\epsilon_p$ controlled cyclic creep acceleration are due to the solute present in the alloy. If this is the case, results presented in this thesis and results presented by Knaus should be consistent. To show the similarity, consider Figure IV-4 which compares a single, low frequency of loading strain cycle, characteristic of Knaus' work, to a segment of higher frequency of loading strain-time data representative of the present work. Both cases should represent, in some way, a repeating cycle of Luders band nucleation and propagation followed by a period of recovery. As discussed earlier, the strain bursts and normal creep portions of the high frequency of loading curve represents this cycle. The strain burst frequency is largely controlled by the recovery rates of the Luders strain hardening observed at that frequency of loading.

The low frequency of loading data presented in Figure IV-4 represents the case where the half cycle time is on the order of the static Luders band frequency. The large strain increment upon reloading, $\Delta\epsilon_p$, in this case represents several Luders bands nucleating and rapidly propagating. The slow upper strain rate reflects the

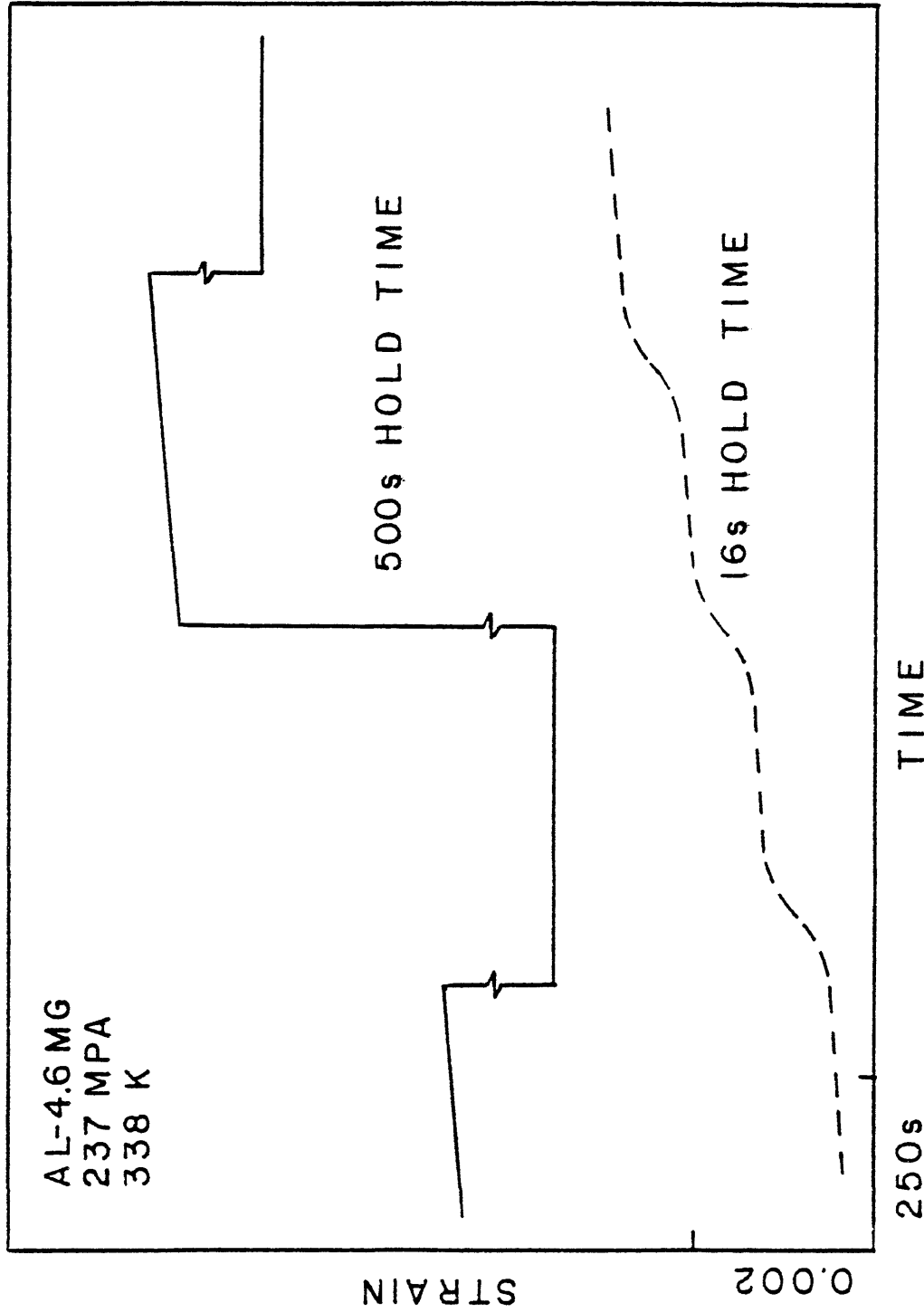


Figure IV-4: A comparison of high frequency of loading cyclic creep behavior (lower curve) to low frequency of loading cyclic creep behavior (upper curve). Test conditions: 338K, 237 Mpa peak stress, 90% load amplitude, 0.027 hz-16 s hold time(lower curve), and 0.001 hz-500 s hold time(upper curve).

work hardened structure that results from this large amount of deformation. The long time period at the lower stress allows sufficient recovery to occur that multiple Luders bands are nucleated upon reloading. In the case shown in Figure IV-4, the $\Delta\epsilon_p$ represents the propagation of about five Luders bands. In this way, the low and high frequency of loading data both represent the Luders phenomena.

Another point brought out in Figure IV-4 is that large substructural changes probably do not occur during cyclic creep in Al-4.6%Mg. The recovery that occurs is relieving the work hardening that is associated with the extensive, localized deformation accompanying a Luders band. If large substructural changes did occur, the upper strain rate would be expected to be faster than the static strain rate. This was not observed at any time in Al-4.6%Mg.

The characteristics of $\dot{\epsilon}$ upper control, however, indicate that large substructural changes are occurring in cyclic creep of pure aluminum. The faster strain rate at the upper stress, as shown in Figure IV-3, indicates that some substructural coarsening does occur. By removing the solute, the possibility of a Luders phenomena and $\Delta\epsilon_p$

control is removed. The enhanced recovery rate can coarsen the substructure rather than relieving the strain hardening associated with Luders band propagation. $\dot{\epsilon}$ upper control is the result of the substructural coarsening.

In summary, the results and discussion presented in this thesis add to the understanding of cyclic creep acceleration. Arguments presented within this work show that there is dynamic interaction between dislocations and solute atoms during creep in the dynamic strain aging temperature range. The effect of cyclic loading is to increase the effect of this interaction which results in cyclic creep acceleration. The different modes of cyclic creep acceleration are more easily understood based on the arguments presented in this thesis.

CHAPTER V

CONCLUSIONS

The following is a brief review of the major conclusions of this work.

1. The strain bursts observed during static and cyclic creep are shown to be the result of inhomogeneous deformation, i.e. Luders bands.
2. The apparent activation energy for Luders band nucleation is equal to 74 kJ/mol for static and cyclic creep. This value compares favorably with the activation energy for the initiation of Luders bands during tensile tests and for vacancy migration.
3. The frequency of Luders band nucleation is faster during cyclic creep when compared to static creep.
4. The increased frequency of Luders band

nucleation during cyclic creep is due to enhanced recovery.

5. Cyclic creep acceleration is the result of the increased frequency of Luders band nucleation that occurs during cyclic creep.
6. The recovery rate during cyclic creep is enhanced by excessive non-equilibrium vacancies generated during cyclic loading and internal stress transients during each loading cycle.
7. Solute effects, ie Luders deformation, are responsible for $\Delta\varepsilon_p$ controlled cyclic creep acceleration.
8. Major substructural rearrangements probably do not occur during cyclic creep of Al4.6%Mg.

APPENDIX I

Correlation of Random Variation in
Static Strain Rate under Constant Conditions.

As noted in Chapter III, a maximum variation of a factor of 2 in the minimum average static creep rates were noted in different samples crept under identical conditions. A limited investigation was undertaken to study this variation.

As shown in Figure AI-1, a correlation between the minimum average static strain rate, $\dot{\epsilon}_s$, and the instantaneous strain observed during loading, ϵ_0 , was made. A trend of increasing $\dot{\epsilon}_s$ with increasing ϵ_0 is observed. A further correlation between yield strength and static strain rate was also made with decreasing yield strengths leading to increasing strain rates. This trend is not graphically shown. While both trends are real, considerable scatter is noted. A slight variation in sample hardness would explain these two trends. If a sample were slightly softer, one would expect both a larger ϵ_0 and a slightly faster average minimum strain rate. These trends are

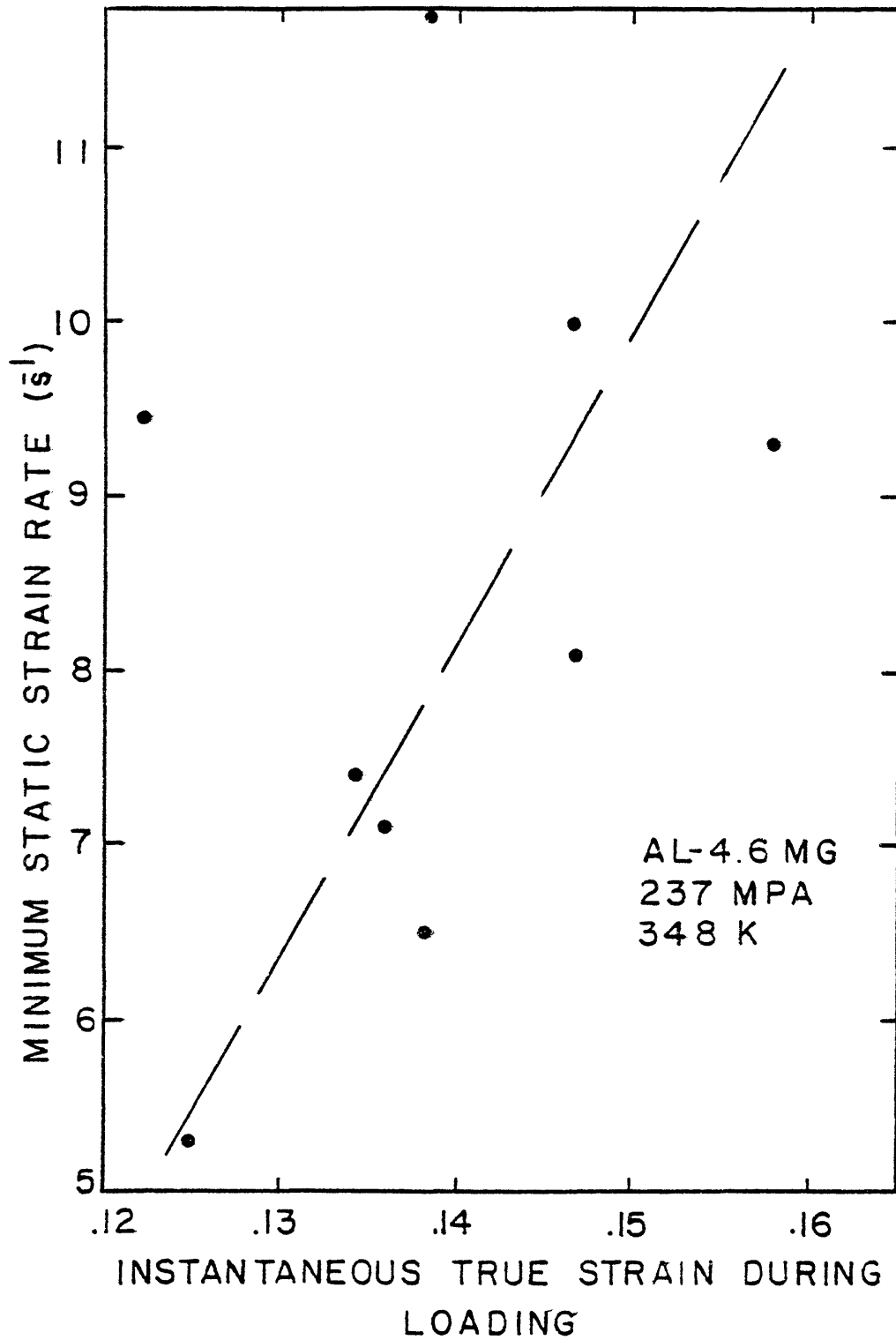


Figure AI-1: The relationship between minimum static strain rate and instantaneous strain during loading observed in various creep experiments at 348K and 237 Mpa.

observed as discussed above. Hardness measurements, Rockwell F, were made to confirm this explanation. Slight variations in hardness were noted, but no valid trends were observed.

It was concluded that slight sample hardness variations were responsible for the observed variations in strain rate. These hardness variations were not measurable by standard hardness testing. The variation in hardness was consistent with observed trends in strain rate compared to both yield strength and ϵ_0 . Attempts were made to correlate the strain rate variation with heat treatment without success. Samples heat treated side by side exhibited these variations.

This limited investigation concluded that the observed variations were due to slight sample hardness variations that were not easily measurable not controllable.

LITERATURE CITED

- August, J. S. 1977. Private communication.
- Baird, J. D. 1971. The effect of strain-aging due to interstitial solutes on the mechanical properties of metals. Metallurgical Reviews. #149. v. 5 p. 1-18.
- Borch, N. R., Shepard, L. A., Dorn, J. E. 1960. Activation energies for creep of a solid solution of magnesium in aluminum. Transactions of the American Society for Metals. v. 52. p. 494-513.
- Brindley, B. J., Worthington, P. J. 1969. Serrated yielding in substitutional alloys. Philosophical Magazine. v. 19. p. 1175-1178.
- Brindley, B. J., Worthington, P. J. 1969. Serrated yielding in Al-3%Mg. Acta Metallurgica. v. 17. p. 1357-1361.
- Cetlin, P. R., Gulec, A. S., Reed-Hill, R. E. 1973. Serrated flow in aluminum 6061 alloy. Metallurgical Transactions. v. 4. p. 513-517.
- Cottrell, A. H. 1953. A note on the Portevin-LeChatelier effect. Philosophical Magazine. v. 44. p. 829-832.
- Coutinho, C. B. 1973. Fatigue-perturbed creep of an aluminum-magnesium alloy at intermediate temperatures. PhD thesis #T-1590. Colorado School of Mines.
- Coutinho, C. B., Matlock, D. K., Bradley, W. L. 1975. Cyclic creep of Al-4.6%Mg at moderate temperatures. Material Science and Engineering. v. 21. p. 239-247.
- Evans, J. T., Parkins, R. N. 1976. Creep induced by cyclic loading in a C-Mn steel. Acta Metallurgica. v. 24. p. 511-515.
- Fiore, N. F., Bauer, C. L. 1967. Binding of solute atoms to dislocations. Progress in Material Science. v. 13. p. 85-134.

- Friedel, J. 1964. Dislocations. Addison-Westley. New York.
- Gibbons, T. B., Herd, J. S., McCartney, L. N., McLean, D. 1973. Creep under varying load. Metal Science Journal. v. 7. p. 196-204.
- Ham, R. K., Jaffrey, D. 1967. Dislocation multiplication, vacancy accumulation, and the onset of jerky flow during forward and reversed strain in Cu-3.2at%Sn. Philosophical Magazine. v. 15. p. 247-256.
- Johnston, W. G., Gilman, J. J. 1954. Dislocation velocities, dislocation densities, and plastic flow in lithium fluoride crystals. Journal of Applied Physics. v. 30. #2. p. 129-144.
- Kennedy, A. J. 1956. Effect of fatigue stresses on creep and recovery. Proceedings of the International Conference on Fatigue of Metals. London. p. 401
- Knaus, S. E. 1975. The effect of stress function variations on the fatigue perturbed creep of an Al-Mg alloy. MS Thesis #T-1779. Colorado School of Mines.
- Langdon, T. G., Mohamed, F. A. 1973. The strain dependence of vacancy creation and dislocation density during serrated yielding. Scripta Metallurgica. v. 7. p. 1199-1204.
- Matlock, D. K., Bradley, W. L. 1976. Fatigue perturbed creep in aluminum and aluminum-4.6%Mg. Proceedings of the Second International Conference on Mechanical Behavior of Materials. Boston. p. 502-506.
- MacEwen, S. R., Ramaswami, B. 1970. Dynamic strain aging and jerky flow in Al-Mg single crystals. Philosophical Magazine. v. 22. p. 1025-1037.
- McCormick, P. G. 1970. The form and initiation of serrated yielding in an Al-Mg₂Si alloy. Philosophical Magazine. v. 23. p. 221-224.

- McCormick, P. G. 1971. Effect of grain size on serrated yielding in an Al-Mg-Si alloy. *Philosophical Magazine*. v. 23. p. 949-956.
- McCormick, P. G. 1972. A model for the Protevin-LeChatelier effect in substitutional alloys. *Acta Metallurgica*. v. 20. p. 351-354.
- McCormick, P. G. 1974. The effect of strain on the aging time for serrated yielding in an Al-Mg-Si alloy. *Acta Metallurgica*. v. 22. p. 484-493.
- McLean, D., Mitra, S. K. 1966. Workhardening and recovery in creep. *Proceedings of the Royal Society of London*. v. 295. p. 298.
- Meleka, A. H. 1962. Combined creep and fatigue properties. *Metallurgical Reviews*. v. 7. p. 43-93.
- Mori, T., Meshii, M. 1969. Plastic deformation of quench-hardened aluminum single crystals. *Acta Metallurgica*. V. 17. p. 167-175.
- Mukherjee, K., D'Antonio, C., Maciay, R., Fischer, G., 1968. Impurity-dislocation interaction and repeated yielding in a commercial Al alloy. *Journal of Applied Physics*. v. 39. p. 5434-5440.
- Mukherjee, K., D'Antonio, C., Maciay, R. J. 1970. On the grain size dependence of the activation energy associated with serrated yielding. *Scripta Metallurgica*. v. 4. p. 209-212.
- Mura, T., Novakovic, A., Meshii, M. 1975. A mathematical model of cyclic creep acceleration. *Material Science and Engineering*. v. 17. p. 221-225.
- Nam, S. W. 1974. A phenomenological theory of fatigue-perturbed and normal creep of an Al-4.6%Mg alloy at high temperatures. PhD thesis #T-1682. Colorado School of Mines.
- Prasad, Y. V. R. K., Sastry, D. H., Vasu, K. I. 1970. Mechanism of low temperature deformation in quenched aluminum magnesium alloys. *Material Science and Engineering*. v. 6. p. 327-333.
- Reed-Hill, R. E., Gulec, A. S. 1975. Concerning the mechanics of Type-A Protevin-LeChatelier plastic flow initiation in Al 6061. *Metallurgical Transactions*. v. 6A. p. 461-466.

- Rising, T. 1977. Private communication.
- Rosen, A., Bodner, S. R. 1966. The influence of strain rate and strain aging on the flow stress of commercially pure aluminum. *Journal of Mechanics and Physics of Solids*. v. 15. p. 47-62.
- Russell, B. 1963. Repeated yielding in tin bronze alloys. *Philosophical Magazine*. v. 8. p. 615-630.
- Seitz, F. 1952. On the generation of vacancies by moving dislocations. *Advances in Physics*. v. 1 p. 43-90.
- Shepard, L. A., Dorn, J. E. 1956. Delayed yielding in a substitutional solid solution alloy. *Transactions of the AIME*. v. 206. p. 1229-1235.
- Sherby, O. D., Burke, P. M. 1968. Mechanical behavior of crystalline solids at elevated temperatures. *Progress in Material Science*. v. 13. p. 325-390.
- Shetty, D. K., Meshii, M. 1975. Plastic deformation of aluminum under repeated loading. *Metallurgical Transactions*. v. 6A. p. 349-358.
- Shetty, D. K., Mura, T., Meshii, M. 1975. Analysis of creep deformation under cyclic loading conditions. *Material Science and Engineering*. v. 20. p. 261-266.
- Thomas, A. T. 1966. The tensile deformation behavior of an aluminum magnesium alloy. *Acta Metallurgica*. v. 14. p. 1363-1374.